AUSTRALIAN NUCLEARS SICENCE & TECHNOLOGY ORGANISATION

LUCAS HEIGHTS RESEARCH LABORATORIES

A High Energy, Heavy Ion Nuclear Microprobe for Ion Beam Research on the Tandem Accelerator at ANSTO

by

David Cohen, Rainer Siegele and Nick Dytlewski

Abstract

A comprehensive review is given on the production and use heavy ion beams with spot sizes of a few μm. The devlopment of a high energy, heavy ion microprobe at ANSTO and its possible applications are discussed.

National Library of Australia card number and ISBN 0-642-59965-3

The following descriptors have been selected from the INIS Thesaurus to describe the subject contents of this report for information retrival purposes. For further details please refer to IAEA-INIS-12 (INIS: Manual for Indexing) and IAEA-INIS-13 (INIS: Thesaurus) published in Vienna by the International Atomic Energy Agency.

KEYWORDS: ANSTO, ANTARES tandem accelerator, beam optics, beam strippers, charge states, elastic recoil detection analysis, heavy ions, ion beams, ion beam analysis, ion microprobe, ion microprobe analysis, ion detection, MeV range 10-100, nuclear reaction analysis, particle induced x-ray emission, quadrupoles, Rutherford backscattering analysis.

EDITORIAL NOTE

From 27 April 1987, the Australian Atomic Energy Commission (AAEC) is replaced by Australian Nuclear Science and Technology Organisation (ANSTO). Serial numbers for reports with an issue after April 1987 have the prefix ANSTO with no change of the symbol (E, M, S or C) or numbering sequence.

Contents

1 Introduction

To exploit advantages of new and emerging accelerator technologies, and to introduce new ion beam research programs relevant to ANSTO, it is proposed to build a high energy, heavy ion nuclear microprobe on the 9 MV Tandem accelerator ANTARES. This state of the art, world class nuclear microprobe will be designed to focus a wide range of ion beam types, from light ions such as protons up to ions as heavy as iodine. The proposed microprobe will be capable of focusing all these ions into beam spots of similar diameters of the order of a few micrometers.

Ion microprobes allow surface imaging of specimens in addition to the depth profiling capabilities of macroscopic ion beams. The surface resolution is determined by the spot size of the ion beam. The feasibility and the wide range of applications for ion microbeams has already been demonstrated with proton and helium microbeams. Nuclear microprobes have significant advantages in terms of sensitivity for elemental analysis over the electron beam microanalysis.

The advantages of ions heavier than helium in nuclear microprobes was first pointed out by Martin[48] in the late 1970's. Very few heavy ion microprobes have been realized since then, because of the limited availability of high energy accelerators and the difficulty of the task. However, because of the progress in technology and the wider availability of high energy accelerators the number of such facilities is expected to increase in the near future. As far as we are aware, there are at least two other heavy ion microbeams in the design phase at the moment. At the time of writing of this report two alternative designs have been considered for the ANSTO microprobe. The first is an improved quadrupole design by Professor Alexander Dymnikov, the inventor of the well tried and tested Russian quadrupole quadruplet, commonly used in existing, light ion proton nuclear microprobes around the world.[40,68] The second is a standard triplet design, which is also frequently used in light ion proton microprobes.

The proposed heavy ion, high energy nuclear microprobe will be a unique, multi-user facility providing new capabilities for ANSTO and the broader Australian research community in many key research fields. It will have applications in biology, medicine, environment studies, and industry. Extended capabilities for ANSTO in the areas associated with accelerator applications include:

- New microprobe imaging and analytical techniques, complementary with existing SEM and SIMS systems at ANSTO.
- New applications to materials and metallurgical research for the study of novel and 'smart' materials on a microscopic scale, the study of the nature of industrial corrosion and wear of surfaces and charged particle activation of strategic materials for research.

- New applications in semiconductor process development, study of particle beam damage in semiconductors, single event upsets, stability of multi-layered electronic microsystems and metallised contacts to microchip structures.

- New applications to arts and archaeology using the ability to non-destructively characterize microscopic samples.

- New applications to life sciences, by characterizations of biological, medical and genetic specimens with spatial resolution of the order of single cell dimensions or better.

- New applications to environmental sciences in the microscopic study of pollutant uptake by animals, vegetation and fine particle atmospheric aerosols.

- New applications to earth and planetary sciences, including geological processes and mineral exploration or in mineralogy and metallurgy where individual grains can be examined in detail.

The unique combination of high energies, heavy ions and improved detection systems on the nuclear microprobe will provide high sensitivity elemental composition and depth profiling information, allowing surface topography and 3D surface reconstruction to be performed on a broad range of materials. The development of this national facility will provide Australian researchers with unique information on microscopic properties of materials.

Currently more than 40 nuclear microprobes are operating worldwide, the vast majority of these are low energy (less than 3 MeV) light ion facilities using proton and helium ion beams. A representative sample of these facilities is given in Table 1. As far as we are aware, there are only six dedicated heavy ion microprobe systems available in the world. These are in Europe, the USA and Japan. Most of these operate on accelerators with terminal voltages below 3 MV. The proposed Australian heavy ion nuclear microprobe would be a world class instrument at the leading edge of current research in this field, operating at terminal voltages from 3 to 10 MV. The world wide increase in the availability of high energy and heavy ion beams has resulted in the development of new and novel ion beam analysis (IBA) techniques. A nuclear microprobe on the ANTARES Tandem Accelerator will allow ANSTO to carry these new developments into the domain of microbeams.

The range of ions and energies available on the proposed ANSTO high energy, heavy ion microprobe is not available on any other microprobe in Australia. Existing ion microprobe systems in Australia are at the University of Melbourne and at CSIRO in North Ryde. The ion beam optics of these microprobes are designed to focus low energy light ion, such as proton and helium. They operate on

GSI[19–21,53]	Germany		LINAC	C - U at 1.4 - 20 MeV/amu
JAERI	Japan	3 MV	Tandem	heavy ions
Sandia[14,15,26,59,61]	U.S.A.	5 MV	Tandem	H, He, Li, Si, N
CSIRO[68]	Australia	3 MV	Tandetron	P, He, PIXE, Imaging
Melbourne[40]	Australia	4 MV	Pelletron	P, He, PIXE, Imaging
Oregon[37,38,66]	U.S.A.	5 MV	single ended	
Bochum[50,51]	Germany	4 MV	Tandem & 400 keV	quadruplet
MPI Heidelberg[4,81]	Germany	6 MV	Tandem	P, He, PIXE
FZ Rossendorf[27]	Germany	3 MV	Tandetron	triplet
FG München[3]	Germany	2.5 MV	single ended	
Upsala[73]	Sweden	6 MV	Tandem	3–4 MeV P
Lund[46]	Sweden	5 MV	single ended	
Oxford[7,8,24]	England	2 MV		
Singapore[84]	Singapore	2 MV	single ended	P, He, PIXE, Imaging
Amsterdam[60,82]	Netherlands	30 MeV	Cyclotron	only P, 2.4-30 MeV
Livermore[26,64]	U.S.A.	10 MV	Tandem	
NAC[62]	South Africa	6 MV	single ended	4.5 MeV He & 2.5 MeV H
Fudan[72]	China		Pelletron	
Dhakran[1]	Saudi Arabia	2.25 MV	Tandetron	
Bruyéres Le Châtel[18]	France			
Louvre Museum[44]	France	3 MV	Pelletron	
GIRO Osaka[29,32,34,55,77]	Japan	1.5 MV	Tandem	

Table 1: Incomplete list of micro beam facilities in the world. The list gives the energy and ion type commonly used.

accelerators with terminal voltages in the range of 1 to 5 MV. The ANSTO microprobe is designed to have a large dynamic range, capable of focusing not only high energy heavy ions, but the full energy range of the ANTARES Accelerator for both light and heavy ions. This universal microprobe design will therefore be complementary to the existing Australian facilities, and will considerably extend the range of accelerator based techniques available to the Australian research community. With its elemental analysis and depth profiling capabilities it will provide valuable information not available from more exotic facilities such as synchrotron X-ray sources, and therefore complements the results from synchrotron radiation experiments.

2 Research Applications

A search of the recent nuclear microprobe literature (see references) shows research applications for these facilities are very broad and far reaching. Microbeam research and its applications have led to a dedicated series of international conferences over the last 9 years. It is difficult to summarize all applications of nuclear microbeams in a brief report, because there are so many of them. The proceedings of the microbeam and ion beam analysis conferences give the best overview of the wide range of applications. A brief summary sorted by various fields is given below.

2.1 Microprobe and Materials and Metallurgical Sciences

In material science, nuclear microprobes can be used both as an analysis tool, or to modify a material. Ion beam modification techniques have been widely used on a great variety of samples (see IBMM conference series). Microbeams add the possibility for localized modifications, which is already widely used for low energy microbeams. Higher energetic ions, however, increase the depth over which the modification takes place. Further they enable novel ion beam modification techniques,[79] because of the different stopping behaviour of the ions.

In recent years, the ion beam modification of high T_c materials using high energetic heavy ion beams, has attracted a lot of attention. High T_c materials irradiated with heavy ions at high energies can tolerate the application of higher magnetic fields before the superconductivity breaks down. This is explained by damage tracks caused by a single ion, that creates an area which is no longer superconducting and thus allows the magnetic field to penetrate into the sample. The creation of localized damaged areas can be applied to various other materials, thus creating novel materials with unique properties. In SiO_2 the refractive index changes because of the damage and thus waveguides can be written directly on a Si-wafer.

As an analytical tool, nuclear microprobes are used to investigate the surface distribution of elements. In metallurgy, where often a variety of phases of an alloy exists in different areas of the same specimen, this opens the possibility of probing localized areas and mapping the elemental distribution over a specimen. Since the energy loss of an ion depends on the number of atoms it penetrates through, nuclear microprobes can be used to probe density variations on a micrometer scale across a specimen. This provides a measure for the homogeneity of a material, which becomes more and more important with the shrinking size of not only of electrical, but also mechanical devices.

2.2 Microprobe and Environmental Sciences

Various accelerator based techniques such as PIXE are already extensively used in environmental studies. The measurement of trace elements in aerosols has become an important application of accelerator based techniques in environmental sciences. With a nuclear microprobe, it will become possible to study the composition individual aerosol particles. This is essential in order to be able to trace the origin of the aerosols.

With nuclear microprobes, the concentration of heavy metals has been measured in the growth rings of shell fish,[11,12] trees,[22] and in deposited ancient ice. This gives valuable historical and seasonal information of environmental pollution. Further, lake sediment chemistry has been studied by Grime and Davison[25] as well as particles suspended in lake waters.[13] McFarlane et al.[45] studied the leaching of aluminium from the weathering profile of the African surface. All these studies were done using nuclear microprobes. They provide valuable information for environmental sciences and will become more and more important, since environmental issues are the major challenge in the future.

Boss et al.[5] have done extensive studies on the longitudinal and radial distribution of major, minor and trace elements in different hair samples. Hyperaccumulation of metals like Co, Cu, Ni Zn and Pb by certain plants is a well-known, but not understood, phenomenon.[52,63] These studies aimed at the understanding of how environmental pollution influences plants and animal life. This is an important question that can be studied with ion microprobes.

2.3 Microprobe and Microelectronics

Ion microprobes have already shown their potential in semiconductor fabrication processes. Examples are two and three dimensional microanalysis of multilevel wiring,[76] self aligned silicides,[78] soft error immunity in DRAMs[65] and maskless processing. RBS and channeling RBS, combined with a microbeam, can provide

non-destructive microanalysis which enables the three dimensional atomic distributions, composition and crystallinity of semiconductor devices to be measured.

In conventional low energy, light ion microprobe applications, the problem of sample damage is considered to be an obstacle. The enhanced reaction cross section of heavy ions enables the analysis of samples using a much smaller ion beam dose and hence considerably reducing the damage in the specimen. However, deliberate damaging can be used to modify the properties of a material and thus fabricating a new material. Using a nuclear microprobe this technique has been used to make optical wave guides by direct ion beam writing.

Soft error immunity of integrated circuits, or the so called Single Event Upset (SEU) imaging, is an example of a low current application for a heavy ion nuclear microprobes. While modern integrated circuits are getting smaller and smaller in their dimensions, they also become more vulnerable to failure because of bombardment by highly energetic cosmic particles. This is of crucial importance for devices used in telecommunications, spacecrafts and spacecrafts control. Hence, soft error mapping and ion beam induced current (IBIC) measurements have attracted a lot of attention from aerospace and high tech companies in recent years. The knowledge gained from nuclear microbeam based research will lead to the optimization of device structures, to improve their radiation hardness. In order attain the energy range of MeV particles that are relevant for cosmic radiation damage, accelerators, such as the ANSTO tandem accelerator, are required.

The size of the beam spot for SEU work has to be in the order of the dimensions of the integrated circuit, with modern circuits having feature sizes of 1 μm or below. Since the required current for SEU is very low, only a few thousand particles per second, these beam spot sizes can easily be achieved with the proposed microprobe.

2.4 Microprobe and Life Sciences

There is a growing need for accurate trace element analysis in the life sciences, because trace elements play a crucial role in the functioning of many proteins and complex biological molecules. About 98% of the human body is made up of nine non-metallic elements. Another 1.89% are formed by the four main electrolytes sodium, magnesium, potassium and calcium. Eleven of the trace elements (Cr, Co, Cu, I, Fe, Mn, Mo, Ni, Se, Sn and Zn) occupy just a tiny 0.012% of the body weight. However this small fraction exerts a tremendous influence on all body functions. These trace elements are required by the cells for normal metabolic processes. Usually the ions of trace elements act as coordination centres for building up or stabilizing the structure of enzymes and proteins. All these elements can be analysed with accelerator based techniques at the ppm level using a nuclear microprobe. A heavy ion microprobe will increase the sensitivity compared to a proton

microprobe and make accessible a wider range of nuclear reaction techniques.

There is a wide variety of analytical techniques that can accurately measure trace elements in biological tissue; these include bulk measuring techniques such as atomic absorption spectrometry (AAS) and inductively coupled mass spectrometry (ICPMS). However, there are very few instruments or techniques that can measure the distribution of trace elements on a microscale. Because of the increasing importance of measuring the elemental distribution at a cellular level, recent emphasis has been placed on the development and use of such instrumentation. There are a few techniques which fall under this classification, such as laser microprobe mass spectrometry, secondary ion mass spectrometry (SIMS), and nuclear microscopy or nuclear microprobe analysis. Elemental analysis using the electron microprobe (EDX), which is currently widely used and very important in the biomedical field, has poor analytical sensitivity of light weight trace elements, particularly those below calcium.

Although the resolution of a nuclear microprobe is not comparable with the resolution of an electron microprobe, there are many important structural features in medicine and biology that cover the range between 1-20 μm. This is demonstrated by the fact that nuclear microprobes have been used to measure the distribution of various elements such as Ca, Cl, Al, Fe, and Ni, to investigate possible contributing factors to neurological diseases such as Alzheimer's and Parkinson's. Elemental analysis of senile plaque cores and neurofibrilar tangles in Alzheimer's disease has also been carried out[36] as well as quantitative mapping of intracellular cations in the human amniotic membrane,[56] and mapping of and detection of anti-AIDS drugs in white blood cells containing heavy metal tracers.[10] Morretto et al.[56–58] have used a nuclear microprobe with which they could achieve intracellular elemental mapping, to study cellular pharmacology.

2.5 Microprobe and the Arts and Archaeology

Ion beam techniques have been used on various archaeological samples as well as paintings and other works of art, because of their non-destructive nature. Many laboratories even built in-air ion beams facilities that allow them apply ion beams to specimens that are either too big or too delicate to be placed in a vacuum chamber. The specimens analysed range from paintings, manuscripts, books, glass ware and pottery. True nuclear microprobe operation, however, requires that the objects to be placed under vacuum, since the size of the ion beam increases in air.

In archaeology microbeams have been used to reveal corrosion processes near the surface of metals, to observe segregation of lead in bronzes and to study inclusions in ores and in the slag resulting from the smelting process. These studies produced important information that allowed archaeologists to draw conclusions on ancient tool making techniques and trade pathes. In paintings, chemical details

of the composition of the pigments can be revealed, and thereby testify as to the origin of the pigments.

In-air systems usually use microbeams of 20-1000 μm, which is quite adequate in most cases in arts and archaeology, where the sample cannot be placed in vacuum. This is still small enough to allow the study of different pigments in a picture, or the print of a book.

The study of ancient pottery is mostly a question of provenancing, i.e. finding the source of the clays that comprise the product of the artisan. The same applies for studies of colour pigments in ancient paintings. Various objects have been studied with nuclear microbeams, such as pottery and glasses, bronze, paintings and pigments, gold and jewellery, manuscripts and paper objects.

2.6 Microprobe and Earth and Planetary Sciences

The nuclear microprobe is the perfect tool for the microanalysis of geological samples, where quantitative trace element analysis and imaging are essential. A major challenge of geology is to deduce the structure and chemistry of the earth's interior from the study of samples collected near the surface. We learn about the processes that shaped the evolution of the crust and the mantle, from the study of the geochemical and petrographic signatures and sequence of geological change recorded in rocks. Microanalytical probes can reveal much about the structure and chemical makeup of the earth from (1), the analysis of samples from the crust and the upper mantle carried to the surface as xenoliths in volcanic eruptions, or tectonically emplaced in the crust and exposed by erosion and (2), the analysis of volcanic magma composition.

For many years, the electron microprobe has been one of the major tools for this research, providing quantitative microanalysis for both major and minor elements. However, many elements of interest are below the detection limit of the electron microprobe. Some trace elements display responses to their chemical and physical environment, and so can provide important new clues for geological research. The advantage of the nuclear microprobe is its higher sensitivity to trace elements inaccessible by other, non-nuclear methods.

The nuclear microprobe can be a very useful tool in geological research if e.g., the composition of an individual crystal has to be probed, rather than the average composition of a geological sample. On a μm to mm scale, the characterization of zoning of trace and major elements reveals information on the chemistry, timing and dynamics of geological processes.

Nuclear microprobe helped to understanding geological crystallization processes, through the study of the distribution of elements in crystal as well as the analysis of ore forming fluids, which can be found trapped as fluid inclusions in minerals. The study of the detailed mechanisms for the growth of minerals and

ore deposits is a very important geological application of the nuclear microprobe, especially in Australia. Various groups have also used the nuclear microprobe to study meteorites.

Recent advances in geological applications include improvements in quantitative PIXE analysis at the trace level, further development of NRA to obtain isotopic ratios and further development of ion luminescence (IL) as a complement to elemental analysis.

3 Microprobe Methods

Progress in materials science, environmental and biological science is strongly dependent on the development and improvement of instruments and techniques for microanalysis and microcharacterization. This is particularly the case with recent trends to miniaturization in materials research and related areas. The proposed microprobe will utilize the high energy, heavy ion capabilities of the ANSTO Tandem accelerator. The microprobe design will enable ion beams up to 100 MeV to be focused to spot sizes of the order of a few micrometers, and thus a broad range of techniques for materials characterization can be performed.

These techniques can be divided into two groups, low current and high current applications, depending on the target current required for the particular technique. The division into these two categories is particularly useful, since the ion current available on the specimen is very closely linked to the beam diameter and hence the surface resolution. The available target current decreases with the beam diameter, and hence much smaller beam spot sizes can be achieved for low current applications compared to high current applications.

Ion beams extracted from a tandem accelerator are often multiply charged. However, in most IBA techniques the number of impinging ions determines the effectiveness of the technique, rather then the electrical target current. The number of impinging ions is often referred to as particle current and is expressed in amps assuming a singly charged particle. In the following discussion, the target current is always assumed to be the particle target current I_p, which is defined as

$$I_p = \frac{I}{q} \tag{1}$$

where I is the electrical current and q is the charge of the current carriers.

The division line between low and high current applications for microprobes can be drawn at around 50-100 pA, with high current applications requiring at least a target current of 50-100 pA in order to be feasible, while for low current applications particle target currents of a few pA or less are sufficient. The current available on target at a given spot size will be discussed in more detail later.

Another way to categories nuclear microbeam applications, is by the information they provide on a specimen. In general, high current applications are analytical techniques that allow an elemental analysis and depth profiling of a specimen. PIXE and RBS are examples of such techniques, both are frequently used in proton microprobes. A target current of 100 pA into a 1 μm spot is generally quoted in the literature as a value that makes both of them feasible.[6] Low current techniques can be characterized as imaging techniques, which include STIM, secondary electron imaging etc. Both groups of techniques supplement each other. A specimen is imaged with a technique of the second group and after-words from the image a particular spot is chosen on which an elemental analysis is performed at an enlarged spot size.

3.1 Microprobe Imaging Techniques

Nuclear microprobes enable a wide variety of imaging techniques. These include scanning transmission ion microscopy (STIM), microtomography, secondary electron imaging and ion beam induced current imaging (IBIC) of devices. All these imaging techniques require target currents of a few pA or less and hence a high lateral resolutions can be achieved. For proton microprobes, lateral resolutions below 0.5 μm[43] have been obtained.

Imaging techniques have proven to be a powerful tools, especially when used in conjunction with the elemental analysis capabilities of ion beams. Imaging techniques have been used i.e. in biomedicine on small insects, plants and parts of animals. In materials science, the homogeneity of thin films, e.g. CVD grown diamond[71] has been measured with STIM. STIM has the capability to measure density changes in materials and can therefore be applied to a wide variety of material science problems. Thin films created by CVD and other techniques can be grown with a very well known thickness, while the density of these films can vary, depending on the growth conditions. STIM provides a tool that can easily measure the density and density variations across the surface.

Various groups have used ion microprobes to image semiconductor devices.[29,75] Various improvements can be made to transmission imaging techniques using the higher ion energies available from accelerators like the FN tandem at ANSTO. The resolution of electron microscopy is limited by multiple scattering of the electrons in the sample, and thus very thin samples have to be prepared. This is a very time consuming and sometimes even impossible. The low energy proton microprobe has already proven its advantage over the electron microprobe by allowing much thicker specimens to be investigated. Using even higher proton energies will allow the imaging of samples as thick as half a mm, thus making the time consuming thinning of samples unnecessary.

The contrast obtained using transmission imaging depends on the energy loss

of the ions. Ions heavier than protons, have a higher energy loss per unit path traveled, which will significantly improve the contrast and thus the ability to determine small density variations. Various groups have already used the advantage of helium ion beams for imaging. Ions even heavier than helium and at higher energies will further improve the contrast of transmission imaging techniques.

3.2 Microprobe Analytical Techniques

Ion beams with small spot sizes are particularly useful to analyse specimens with a microstructure. Nuclear microprobes provide these small spot sizes and can generally be used to investigate non-uniformities in the composition of specimens that occur on a scale below 0.1 mm. Due to the surface resolution of microprobes three dimensional elemental profiling becomes possible if one of the depth sensitive ion beam analysis (IBA) techniques is used.

IBA techniques involve interactions between the energetic ion and the nuclei and electrons of the target atoms. These interactions can lead to the scattering of the energetic ions and target atoms as well the excitation of the target atoms. In Rutherford Backscattering Spectroscopy (RBS), the energy of the scattered ions is the detected, while in Elastic Recoil Detection Analysis (ERDA), the scattered targets atom are detected. Both techniques are depth sensitive, since the energy of the detected particle is a function of the depth. Interactions between the incident ion and target electrons give rise to characteristic X-ray or light emission. The characteristic X-ray emission is used in Particle Induced X-ray Emission (PIXE), while the light emission called Ionluminescence (IL) has recently attracted attention, because it allows the detection of rare earth elements with a high sensitivity.[28,85,86] If the ion energy is high enough to penetrate the coulomb barrier of the nucleus, nuclear reactions occur which are used in Nuclear Reaction Analysis (NRA), or Particle Induced Gamma Emission (PIGME) analysis. All ion beam techniques can be utilized with an ion microprobe, thus allowing surface mapping of the elements.

An analysis technique can be considered viable with an ion microprobe, if it can be performed within a few of hours under standard conditions. In IBA, this means the count rate has to be high enough to acquire sufficient information over the measurement time. The count rate is proportional to the available beam current and the reaction cross section. Compared to IBA using conventional macroscopic ion beams, the target current in a nuclear microprobe will be as much as 3 orders of magnitude lower, depending on the spot size. This means other factors (such as the cross section) have to compensate for the lower target current. Fig.1 shows the cross sections of common IBA techniques, such as RBS, ERDA and PIXE. The cross sections of these techniques generally exhibit a smooth behaviour as a function of the ion beam/target mass combination, and ion beam energy.

The cross sections in NRA depend strongly on the specific reaction used and thus no general trend can be shown. However, some reactions, principally involving light elements, have high cross sections at higher energies, that are only accessible with accelerators such as the ANSTO Tandem Accelerator. Fig. 1 demonstrates, that the cross sections for the various ion beam analysis techniques vary by more than 7 orders of magnitude for light mass elements, while the variation for medium to heavy mass targets is much smaller, typically 4 orders of magnitude. Hence, the choice of the analysis technique depends on the type of material under investigation. In general, cross sections with a value greater than 1 b/sr are required for a viable method for analysis in an ion microprobe.

The count rate C in a detector is proportional to the differential cross section $d\sigma/d\Omega$, the beam current I, the detection solid angle Ω, and the detector efficiency ϵ, i.e.

$$C \propto \frac{d\sigma}{d\Omega} I \Omega \epsilon \tag{2}$$

PIXE X-ray detectors have an efficiency ϵ between 1% and 100%, depending on the X-ray energy, while the efficiency for particle detection in ERDA and RBS is close to 100%. The detector solid angle Ω depends on the geometry and the size of the detector. X-ray detectors typically have solid angles of 10 msr, while standard RBS and ERDA solid angles are in the order of 1 msr.

Equation 2 suggests different ways in which the feasibility of a particular technique can be improved. One is via the cross section, while another is through the detection angle. In RBS larger detector solid angles can be achieved using an annular shaped detector, while in ERDA, position sensitive gas detectors,[2] can achieve a similar improvement.

Fig. 2 shows the expected count rate per pA derived from the reaction cross sections shown in fig. 1 using the equation 2. Fig. 2 allows a comparison between different techniques. However, for some techniques other factors like the background etc. also influence their feasibility.

Another way to check the feasibility of a technique is to estimate a typical analysis fluence and the maximum analysis time one is willing to accept. From this the required target current can be calculated. Table 2 shows the analysis fluence of a typical ERDA with I, He-RBS and H-PIXE. The fluences required for these techniques using different ions can be obtained by scaling these values by the cross sections. The table also gives a minimum target current assuming a maximum analysis time of 1000 sec. The table shows that a minimum target current of 300 pA is required for any of these analytical techniques to be feasible.

However, it should be mentioned that these values can be improved by increasing the detection solid angle or for example by increasing the cross section. In the case of ERDA using the same ion, the cross section can be increased by lower-

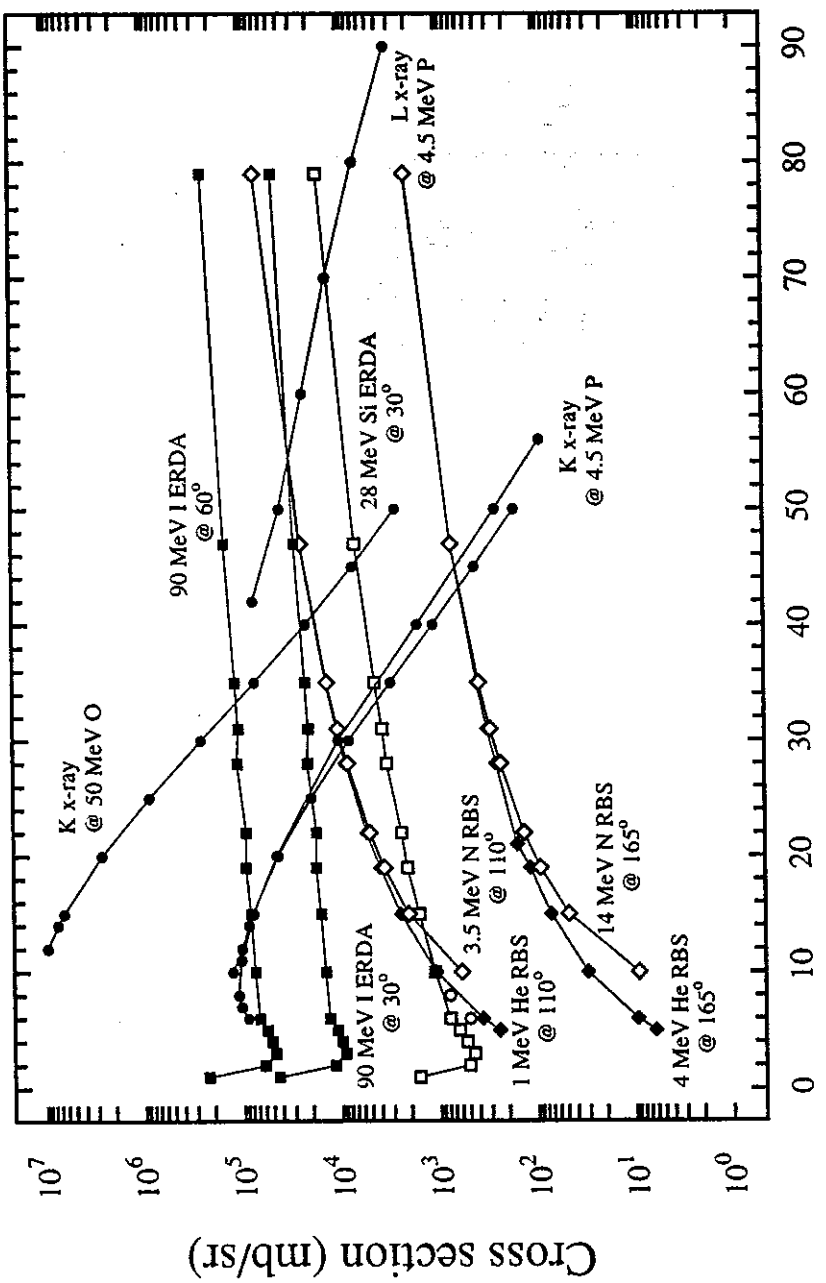

Figure 1: Cross sections for various ion beam analysis techniques.

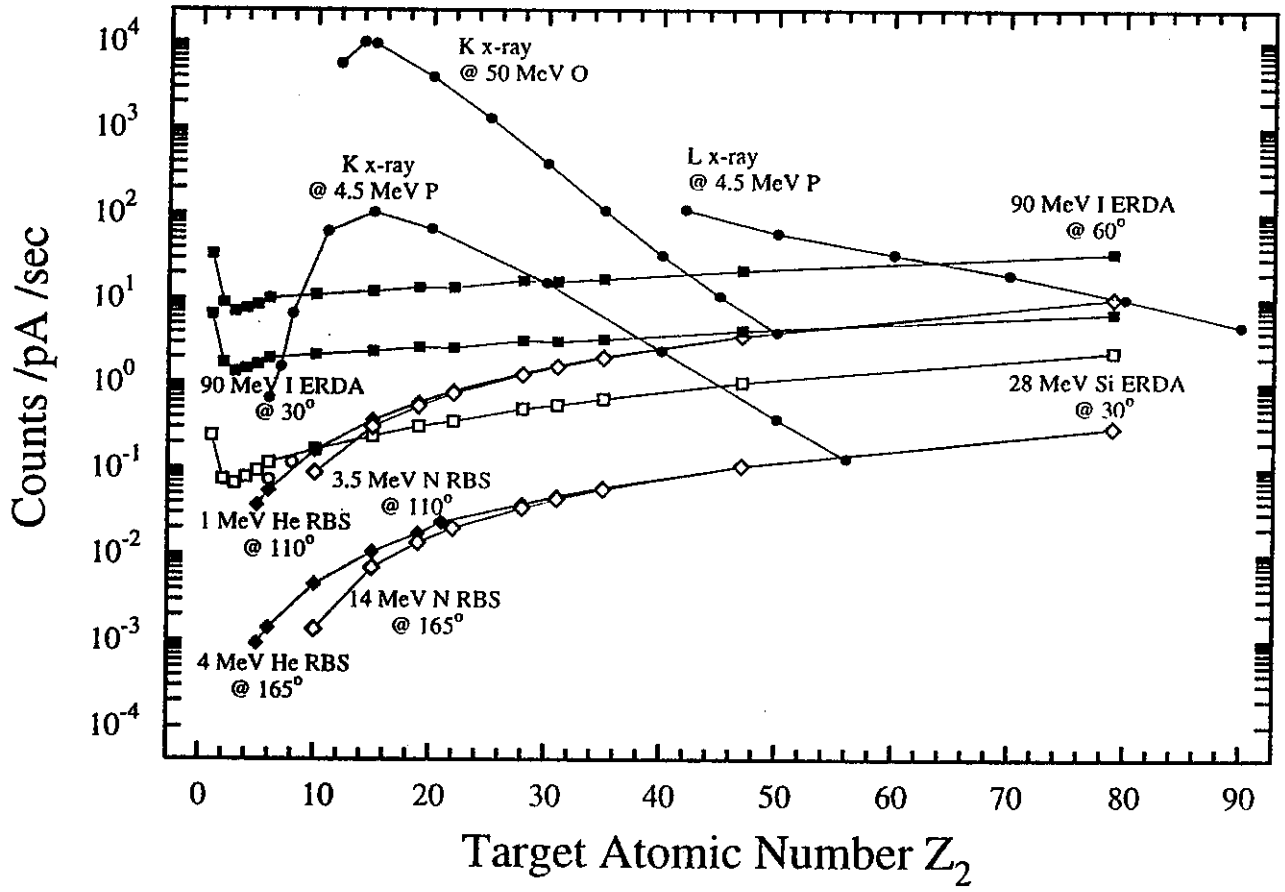

Figure 2: Counts/pA/sec for various ion beam analysis techniques.

Table 2: Typical values for the analysis fluence in RBS, ERDA and PIXE. The table also gives the minimum analysis current that allows such an analysis to be performed in 1000 sec or less.

	Analysis fluence μC	min. target current nA
I-ERDA at 30°	0.3 - 3	0.3 - 3
He-RBS at 165°	1 - 10	1 - 10
H-PIXE	0.3 - 5	0.3 - 5

Table 3: Ranges, straggling and lateral spread of various ions in carbon at typical ion energies.

Ion	Energy MeV	Stopping Power keV/μg/cm^2	Range μm	Range Straggling % total	lateral Spread % total
e^-	0.05	0.006	10	100%	100%
H	2	0.14	37	3.9%	4.5%
H	10	0.04	595	4.5%	3.9%
He	2	1.4	5	3.4%	4.6%
He	10	0.5	55	4.2%	2.3%
Cl	50	23	11	3.0%	2.8%
Br	60	46	9	3.1%	4.6%
I	90	60	11	3.1%	4.4%

ing the ion energy or increasing the recoil angle. Both, however will decrease the detection depth.

3.3 Advantages of High Energy, Heavy Ion Beams

The ANSTO heavy ion microprobe will not only provides light ions, but wide range of ions at different energies, which results in a variety of advantages. The cross section for the ERDA and PIXE techniques increase proportionally to the square of the nuclear charge of the ion probe, Z_1^2. This can be seen from the PIXE cross sections for protons and oxygen ions, as well as the ERDA cross sections for silicon and iodine ions in fig. 1. The higher cross sections for heavy ions enables a much enhanced analysis sensitivity. This gives a high energy, heavy ion microprobe a major advantage over the more conventional low energy, light ion (proton) nuclear microprobes.

The depth resolutionăand maximum probing depth are important parameters for the performance of an analytical technique. In ion beam analysis and microprobe applications both are related to energy loss of the ion and the ion range. Table 3 shows these values together with the range straggling and the lateral spread of various ions in a carbon matrix at typical ion energies. As a comparison, the values for electrons at 50 keV, a typical energy in electron microscopy, are also given. Because of their small mass, electrons get deflected significantly in collisions with the nuclei and electrons of the target atoms. This is the reason for the large values for the range straggling and the lateral spread.

As indicated in table 3, there is a ten fold increase in stopping power between H and He at energies of 2-10 MeV, with a further increase by two orders of magnitude for iodine at 90 MeV. In nuclear techniques, such as RBS, ERDA etc., the depth resolution depends strongly on the energy loss and hence, the depth resolution is greatly enhanced for heavy ions. Further, in imaging techniques such as STIM, where the contrast of images is caused by the energy loss, much better contrasts can be achieved.

The range straggling in column 5 gives the variation in range, while the lateral spread gives the average deviation from a straight trajectory. These values do not vary much for the different ions. However, they are significantly less than for electrons used in TEM. This indicates that for a heavy ion microprobe the same, good surface resolutions can be achieved as for light ion microprobes.

The majority of proton nuclear microprobes use the PIXE technique for multielemental analysis. The sensitivity of PIXE is limited by the background X-rays. Three major processes contribute to the background, which are (1) the bremsstrahlung of the primary ion, (2) the bremsstrahlung of secondary electron and (3) Compton scattering of gamma rays produced by nuclear excitations.

The bremsstrahlung of the primary ion is greatly reduced for heavy ions compared to H, thus giving an increased sensitivity. This effect has been shown by Watson et al.[83]

The secondary electron bremsstrahlung contributes a background with a maximum endpoint energy E_{max} given by

$$E_{max} = \frac{2.2}{M} E \quad (\text{keV}) \tag{3}$$

where M is the mass of the probing ion (amu), and E its energy (MeV). For 3 MeV protons this background extends up to 6.6 keV (spectral peaks of iron), but for a 10 MeV oxygen beam, it extends only to 1.4 keV (spectral peaks for aluminium), thus reducing the background considerably. This background reduction could also be achieved by using a proton beam at a lower energy than 3 MeV, however the cross sections and hence the count rate would be much lower. Horino et al. have

shown that, with a heavy ion beam, light elements can be measured with an enhanced sensitivity.[30,31]

Heavy ions also have the advantage of a much reduced gamma ray induced background. The number of gamma rays produced depends strongly on the composition of the target and the ion used. In using light ion beams, their low nuclear charge permits close encounters with the nuclei of the target materials, and so nuclear excitations can result with the production of gamma rays from (p,p'γ) and (p,$\alpha\gamma$) reactions. These gamma rays Compton scatter in the X-ray detector, depositing some energy which appears as noise. The heavier the ion probe, the less this effect becomes. This demonstrates that the choice of heavy ions has a big advantage in PIXE, not only by the increased reaction cross section, but also by the better signal to background ratio.

ERDA and RBS are techniques employing different aspects of the same basic reaction process. When the incident ion beam probe has a collision with a target nucleus, the target nucleus is always knocked in a forward direction. The measurement of the energy of this forward recoiled nucleus is the basis of the ERDA technique. After the collision, the incident projectile can scatter in a backward direction, and it is the measurement of the ion beam's backscatter energy which is the RBS technique. In both cases, information is obtained on the sample composition as a function of depth. These two techniques are complementary, their suitability dependent on sample composition and structure.

As the mass of the ion probe increases, kinematic considerations dictate that after the collision, both scattered nuclei will move in the forward direction. Hence only for heavy ions ERDA becomes an universal tool, that can detect both light and heavy elements. The ion scattering cross sections for ERDA is proportional to the square of the atomic number of the ion Z_1^2, thus leading to an increasing yield for heavy ion beams. This gives heavy ions a great advantage in ERDA.

Although the heavy ion RBS cross-section is slightly lower than that for the standard helium ion probe, it has the intrinsic advantages of a much enhanced depth resolution, and the ability to discriminate better between sample elements of near atomic weights. The RBS cross sections a 4 MeV He ion beam, and a 14 MeV N beam are shown in fig. 1, as well as the ERDA cross sections for a 90 MeV I beam, and a 28 MeV Si beam.

The cross sections in ERDA increases strongly for heavy ions, even at constant ion velocity, i.e. at higher energies. In fact, ERDA becomes a truly universal technique with heavy ions, allowing the detection of all elements from hydrogen up to the mass of the ion or even higher. In contrast, PIXE is normally limited to target elements heavier than aluminium and gives no depth information, while RBS is best suited for the depth profiling of medium to heavy weight elements in a light element matrix. The possibility to use ERDA makes a high energy, heavy ion nuclear microprobe a universal tool, that can be used for the depth profiling of heavy

and light elements simultaneously.

4 The Nuclear Microprobe Design

The performance of an ion microbeam is determined by the probe-forming system of the microprobe. There are two ways of producing a small beam diameter, either by simple collimation of the beam or by using a lens system which demagnifies the ion beam passing through an object aperture. With collimation, the angular divergence of the beam passing through the collimating aperture must be sufficiently small so as to minimize the spreading before it hits the target. This limits the minimum spot diameter with this technique to about 25 μm. A further disadvantage of this technique is that only very small beam currents are achievable.

The production of nuclear probes of less then 25 μm in diameter requires a focusing system that demagnifies the beam emerging from an object aperture. The minimum spot size of a microprobe and the target current, are indicative of the performance of the system. Any microprobe system has to be optimized to produce the highest target current at the smallest spot size.

4.1 Ion Beam Optics

The efficient injection of a beam of particles from an ion source into an accelerator and the transportation of the accelerated beam to the experiment, for example a nuclear microprobe, requires the knowledge of several beam-optical parameters. These parameters are the emittance ε and the brightness β, or their normalized equivalents ε_n and β_n. The emittance ε describes the size and the divergence of the ion beam and therefore defines the beam quality. In a nuclear microprobe the emittance of the ion beam is an important factor, because it influences the performance of the system.

An ion beam particle is completely defined by its position (x, y, z) and momentum coordinates $(p_x,\ p_y,\ p_z)$. By convention the coordinates x and y are, defined as those transverse to the beam direction, while the z coordinate is longitudinal. A particle in the ion beam can thus be represented by a position in a six dimensional phase space. The whole beam of particles is then represented by a group of points in this phase space. The volume the beam particles occupy in the six dimensional phase space is the emittance of the beam. In one plane, for example $(x,\ p_x)$, the beam is characterized by the area A it occupies. The emittance is then defined as

$$\varepsilon = \frac{A}{\pi}. \tag{4}$$

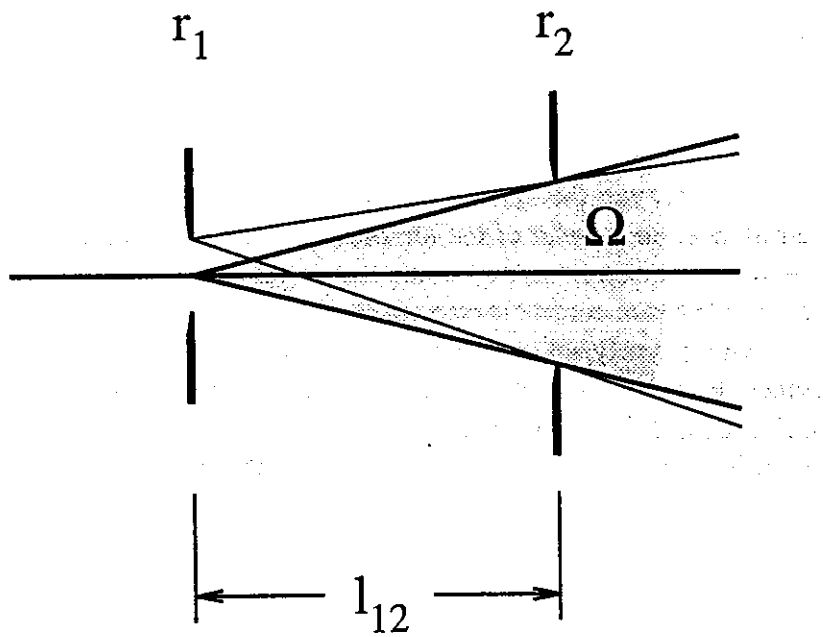

Figure 3: Definition of the emittance.

A more practical definition of the emittance is given by

$$\varepsilon = \frac{\sqrt{2\Omega S}}{\pi}, \tag{5}$$

with the solid angle Ω and the source area S. The beam emittance can experimentally be defined by a set of two apertures with radius r_1 and r_2 separated by the distance l_{12} as indicated in figure 3. The emittance can then be written as

$$\varepsilon = \sqrt{2}\,\frac{r_1 r_2}{l_{12}}. \tag{6}$$

When the ion beam progresses through a beam line the z coordinate of the particles changes, however, the volume the beam occupies in phase space stays constant. This is the essence of the Liouville theorem, which say; the density of the particles in the six dimensional phase space is invariant in time. However, the beam emittance is only constant if no accelerating fields are applied, i.e. the axial momentum p_z does not change. Hence, in an accelerating field the normalized emittance is introduced as a new constant. The normalized emittance ε_n is defined as

$$\varepsilon_n = \varepsilon\sqrt{E}, \tag{7}$$

where E is the kinetic energy in MeV.

The beam emittance is a parameter that determines the matching of an ion beam emitted from an ion source, or the beam transport system, with the experimental apparatus. The geometrical input to some experimental apparatus, for example an ion microprobe, is described by the acceptance of the system. Both the ion beam emittance and the system acceptance have to match in order to permit a high transmission through the system. If the system acceptance is smaller than the beam emittance, only a part of the ion beam passes through the apparatus. A mismatch between the beam emittance and the acceptance of the microprobe decreases the available beam current on the specimen.

Alternatively, an ion beam can be described by its brightness. While the emittance defines the quality of an ion beam in terms of its width and divergence, the brightness defines how many particles are within a certain volume in the six dimensional phase space. The brightness is defined as

$$\beta = \frac{I}{\Omega S}, \tag{8}$$

with the beam current I. The relation between brightness and emittance is then

$$\beta = \frac{2I}{\pi^2 \varepsilon^2}, \tag{9}$$

and the normalized brightness is defined as

$$\beta_n = \frac{2I}{\pi^2 \varepsilon_n^2}. \tag{10}$$

This equation allows the beam current available on target to be calculated. The ion beam current is a function of the beam brightness β and the acceptance ε of the system the beam is passing through

$$I = \frac{\pi^2 \varepsilon^2 \beta}{2}. \tag{11}$$

This equation shows that in order to achieve a large beam current, a high brightness beam or a large system acceptance are required. Since the ion beam brightness is determined by the ion source and the accelerator, it cannot be increased easily. Hence a large system acceptance is required, in order to achieve a large target current.

4.2 Ion Beam Focusing Systems

In order to achieve small probe diameters together with a high target current a focusing system is required. Lens systems currently used in nuclear microprobes can

be divided into two groups according to the underlying physical principle, electrostatic and magnetic lenses. Although electrostatic lenses have a very simple design, they have to be machined with a very high precision and the voltages required to focus high energy heavy ions are very high. Additionally, in electrostatic quadrupoles the chromatic aberration is greater by a factor of two than in magnetic quadrupoles.[23]This excludes electrostatic systems for a heavy ion microprobe.

Magnetic lenses can be divided into two groups cylindrical lenses and quadrupole systems. In electron microprobes and low energy ion probes focusing elements with a cylindrical symmetry are generally used. Cylindrical lenses have the advantage that their ion beam optics is relatively easy and well understood. The focusing action of these elements is created only by the fringing field. This makes it difficult to produce strong enough fields to bend high energetic heavy particles. Only superconducting cylindrical lens systems can create the fields required to focus MeV ions.[50] This leaves the magnetic quadrupole lens as the best choice for a heavy ion nuclear microprobe.

4.3 The Quadrupole Lens

Most existing nuclear microprobes are based on quadrupole lenses. Magnetic quadrupole lenses exhibit a strong focusing action and differ from cylindrical lenses in that the field lines are at right angles to the direction of the ion motion and hence the magnetic field force on the particle trajectory is necessarily greater. In a quadrupole the field components are such that the x-component of the magnetic field is proportional to the distance from the central axis in the y-direction and the y-component of the magnetic field is proportional to the distance from the axis in the x-direction

$$B_x = G_m Y \tag{12}$$

$$B_y = G_m X \tag{13}$$

A pure quadrupole field is derived from a quadrupole lens showing exact fourfold symmetry, with a hyperbolic pole-shape of infinite extent. The action of a quadrupole field on a charged particle passing through the lens is a shown schematically in fig. 4. The forces on a positively charged particle passing down into the paper at the positions 1 and 2 are in a direction towards the central axis and so in the y-plane there is a converging or focusing action. Moreover, the further away the particle is from the central axis the greater the magnitude of the converging force. The forces on a charged particle at the positions 3 and 4 are such that the particles are moved away from the central axis and hence in the x-plane there is a diverging or defocusing action.

From this it is clear, that one quadrupole lens is insufficient to focus a charged particle beam in both planes simultaneously and therefore at least two quadrupoles

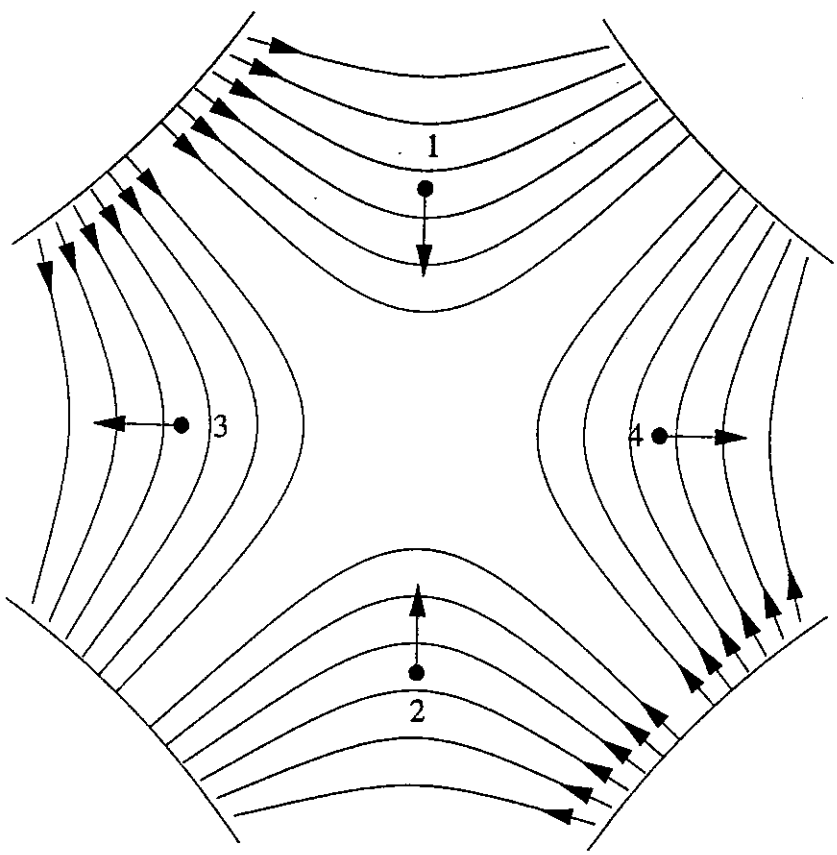

Figure 4: Magnetic field of a quadrupole lens.

with opposite polarity are required in order to focus an ion beam down to a small spot size.

4.4 Magnetic Quadrupole Fields and Ion Beam Rigidity

Most existing microprobes are designed to focus low energy light ions such as 4 MeV H or 2 MeV He. The proposed ANSTO microprobe, in contrast, will be able to focus a wide range of different ions to almost the same beam spot sizes.

A heavy-ion, high-energy microprobe introduces three new parameters, for which the microbeam design has to optimized. These are the ion mass, the ion energy and the charge state of the ion. Fortunately, for considerations concerning the design of the microprobe, these parameters can be reduced to a single parameter, the magnetic rigidity, which is defined a ME/q^2. Ions with the same magnetic rigidity have the same trajectories in a magnetic field. Thus a nuclear microprobe with a magnetic lens system will have the same focusing properties for ions with the same magnetic rigidity. Furthermore, two different ions (1 and 2) will have the same trajectories if the ratio of the magnetic fields is equal to the ratio of the square root of their magnetic rigidities.

$$\frac{B_1}{B_2} = \sqrt{\frac{M_1 E_1/q_1^2}{M_2 E_2/q_2^2}} \tag{14}$$

Hence the quadrupole field required to focus an ion beam, increase with the square root of the magnetic rigidity $(ME)/q^2$ of the ion.

The maximum field that can be obtained in the focusing quadrupoles thus determines the energy and elemental range over which the nuclear microprobe can be used. The ANSTO ion microprobe will be designed to focus beams with a magnetic rigidity up to 110 amu MeV/e^2, which is equivalent to 85 MeV I^{10+}.

From the above, it is obvious, that the limiting factor in the design of a microprobe suitable for both heavy and light ions, is the upper limit of the magnetic field in the quadrupoles. For a 30 cm quadrupole lens this limit is approximately 3 kG. With a more sophisticated technology this limit may be slightly higher. However, we will use 3 kG as a maximum value for the magnetic field throughout the following discussion. The results obtained with this value can easily be scaled for higher maximum fields.

A quadrupole lens has a magnetic field which is zero at the centre, and has a maximum at the pole tips. The gradient G_m of magnetic field in a quadrupole is defined as

$$G_m = \frac{B_p}{r_0} \simeq \frac{2\mu_0 nI}{r_0} \tag{15}$$

with the pole separation r_0, B_p the field at the pole tip and nI the total ampere-turns per pole. This shows that, for the same magnetic field gradient G_m the magnetic

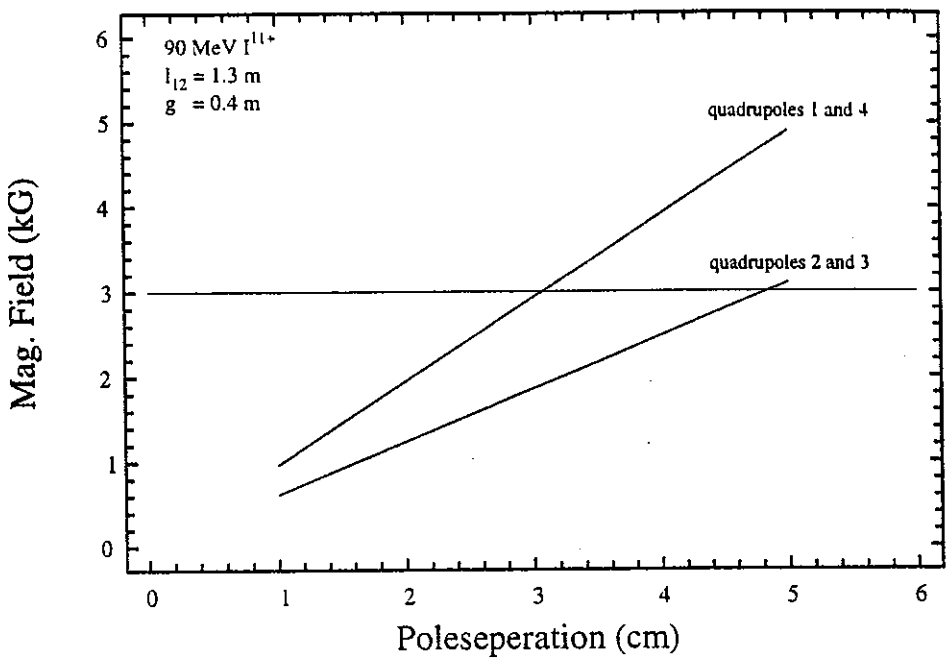

Figure 5: Magnetic field strength as a function of pole separation.

field at the pole tips is proportional to the pole separation r_0. As a consequence, the field strength at the pole tips has to increase, if the separation of the pole tips increases. Hence, excessive magnetic fields in the quadruples can be avoided, if the pole separation is kept as small as possible.

Fig. 5 shows, for a fixed microprobe design, the magnetic field at the pole tips as a function of the pole separation, for a 90 MeV I^{11+} beam. The two lines show the magnetic fields in the two quadruples of the pair. The horizontal line indicates the limit of 3 kG for 30 cm quadrupole lenses. It can be seen that in order to stay within the limit for the magnetic field the pole separation must not exceed 3 cm for this particular design.

The required magnetic fields depend strongly on the geometrical design and the focusing properties of the nuclear microprobe. In general, microprobe designs with stronger focusing properties and thus larger demagnifications require higher magnetic fields. This means the pole separations has to be small in order to make these designs possible within the limits of a 3 kG field. A minimum pole separation of around 1-2 cm is required in order to construct an evacuated beamline through the quadrupole lenses. Smaller pole separations increase the effort required to build an evacuated beamline through the poles. However, a pole separation smaller than 1 cm makes designs with better focusing properties possible.

At a given terminal voltage a spectrum of charge states can be extracted from a tandem accelerator. The maximum and the width of the charge state distribution depends on the stripper medium. As shown above, the upper limit of the field in a magnetic quadrupole determines the maximum value for the magnetic rigidity of an ion beam that can be focused. However, ion beams with the same energy but a different magnetic rigidity, can be extracted from the accelerator, depending on terminal voltage and the charge state of the ion. A 90 MeV I beam can have a magnetic rigidity of 80 or 140 for a charge state of 9 or 12, respectively. This is almost a factor of two difference and demonstrates the influence of the charge state distribution on the microprobe design. In general it can be said that a charge state as high as possible is highly desired.

4.5 Optical Calculations

As shown before, at least two magnetic quadrupoles lenses are required to focus an ion beam in both the x and y plane. In practice, combinations of two, three and four lenses have been used in nuclear microprobe systems. Since there are many possible combinations of quadrupoles, it is necessary to develop a theoretical method that can handle different quadrupole systems for microprobe applications. Such a program was developed by A. Dymnikov at ANSTO.[17]

The starting point for any beam optical calculation is the differential equation of motion of a charged particle in electromagnetic fields. This equation is difficult to solve analytically and even direct numerical solutions are very time consuming. Thus an approximate solution of the equation of the motion for a quadrupole of arbitrary length and excitation is embodied in a matrix **M**, which transforms the ray coordinates at the entrance of the quadrupole to those at the exit. This matrix is known as the transfer matrix and the transfer matrix of a complete system is found by a series of matrix multiplications.

The coordinates of a particle emerging from an optical system may be expressed in terms of the entrance coordinates

$$x_f = m_{11}X_i + m_{12}y_i + m_{13}\theta_i + m_{14}\phi_i + m_{15}\delta + \cdots \quad (16)$$

$$y_f = m_{21}X_i + m_{22}y_i + m_{23}\theta_i + m_{24}\phi_i + m_{25}\delta + \cdots \quad (17)$$

$$\theta_f = m_{31}X_i + m_{32}y_i + m_{33}\theta_i + m_{34}\phi_i + m_{35}\delta + \cdots \quad (18)$$

$$\phi_f = m_{41}X_i + m_{42}y_i + m_{43}\theta_i + m_{44}\phi_i + m_{45}\delta + \cdots \quad (19)$$

$$\delta_f = \delta + \text{higher order terms} \quad (20)$$

where the subscript i refers to the entrance coordinates and f to the exit coordinates. x and y are the x and y coordinates, while θ and ϕ are the divergence in the x and y plane and δ is the energy variation of the particle. The matrix elements

$m_{11} =< x|x >$ and $m_{22} =< y|y >$ for example represents the first order magnifications in x and y.

Aberrations enlarge the focused image of the object aperture. The second order chromatic aberration is derived from the first order matrix elements by taking the energy spread of the beam into account. The second order aberration coefficients are $< x|x\delta >$, $< x|\theta\delta >$, $< y|y\delta >$, $< y|\phi\delta >$, $< \theta|x\delta >$, $< \theta|\theta\delta >$, $< \phi|y\delta >$ and $< \phi|\phi\delta >$. The third order spherical aberrations account for variations of the image position with the entrance angle of the rays, and the aberration coefficients are the higher order matrix elements $< x|\theta^3 >$, $< x|\theta\phi^2 >$, $< y|\theta\phi^2 >$, and $< y|\phi^3 >$.

The vector (x, y, θ, ϕ) represents the size and divergence of the beam, which is the beam emittance or better, in this case, the system acceptance. The challenge in ion microprobe technology is to optimism the optical system in such a way that a small beamspot sizes is achieved for a large system acceptance. This will result in a maximum beam current on the target. However, as can be seen the system acceptance and the spot size are related through the various aberrations of the beam-optical system. In order to minimize the influence of aberrations on the spot size, ion beam particles with trajectories significantly effected by aberrations are removed. This is done by reducing the system acceptance.

The influence of aberrations on the spot size can accurately be assessed by using the Matrix-method. However, G. Legge[43] gives a numerical expression for the spot size due to the chromatic aberration

$$d_c = 2C_c \left(\frac{dE}{E}\right)^{\frac{1}{2}} \left(\frac{I}{\pi^2 \beta_n E}\right)^{\frac{1}{4}} \tag{21}$$

where C_c is the chromatic aberration coefficient, E the beam energy, and dE/E the energy spread. The equation shows, that at a given brightness, the minimum spot size is limited by the required target current. The chromatic aberration coefficient is in the best case equal to the focal length of the magnetic lens. For a typical low energy microprobe with a 3 MeV proton beam and 100 pA beam current this restricts the minimum spot size to 0.2 μm. For the spherical aberration a similar expression for the maximum resolution can be given

$$d_s = \left(\frac{16}{27}\right)^{\frac{1}{8}} \times 2\, C_s^{\frac{1}{4}} \left(\frac{I}{\pi^2 \beta_n E}\right)^{\frac{3}{8}} \tag{22}$$

where C_s is the spherical aberration coefficient. For the same parameters the spherical aberration restricts the resolution to a value of 0.4-0.6 μm.[43]

Both the chromatic and spherical aberration coefficients of a lens or lens system are in the best case proportional to the focal length f of the lens.[42] Therefore it is

always an advantage to use a lens with a small focal length. However, in the case of high energy, heavy ions it is not possible to build a lens with the same focal length as that for protons, because the required magnetic fields would be too high. Further, the brightness of an ion beam extracted from a tandem accelerator is at least 2 orders of magnitude lower compared to the brightness of a single ended machine. This is due to the stripping process at the terminal. Therefore the minimum spot size for a given current of a high energy heavy ion microprobe is expected be by a factor 10-100 larger, depending on the energy and the ion species.

From the equations of the chromatic and spherical aberration it can be seen, that in principle very small spot size can be achieved, however, with a very small target current. Since $2I/(\pi^2\beta_n)$ is the square of the emittance, the minimum spot size is a function of the beam emittance or better the system acceptance. The relation between the emittance and the spot size is shown in fig. 6. The figure gives calculated spot sizes at a given emittance for various microprobe designs. The data shown in the figure are results of 3rd order calculations using the program designed by Dymnikov.[17] The figure further shows very little variation for various designs.

Besides the chromatic and spherical aberration the spot size increase due to other aberrations, that depend on the homogeneity of the materials, the stability of the quadrupole power supplies and the quadrupole alignment which are more difficult to take into account. Excitation aberrations are caused by instabilities in the power supply of the quadrupole lenses, and sextupole field aberrations are caused by a lack of symmetry and uniformity in the lens construction, or the lens material. These aberrations are difficult to account for and therefore the enlargement of the spot size is difficult to predict.

4.6 The ANSTO Tandem Accelerator Facility

The ANTARES Accelerator facility consists of a FN Tandem Accelerator from High Voltage Engineering Corporation. The Accelerator was purchased from Rutgers University and installed at the Lucas Heights Science and Technology Centre in 1989. The accelerator is currently equipped with a belt charging system. Belt charging systems are know to result in a larger energy instability compared to that of pelletron systems. The stability so far achieved at the accelerator is ± 1 kV at 7 MV. This is 0.015% and a standard value for electrostatic accelerators.

The accelerator has recently been upgraded with a gas stripper channel. This allows the extraction of ion beams with a much higher brightness from the accelerator, since multiple scattering is much reduced compared to that from a foil stripper. Additionally the SF_6 pressure in the tank was increased allowing higher terminal voltages, which will further increase the brightness.

In fig. 7 the existing beamline system on the tandem accelerator is shown. The figure shows the already existing beamlines for accelerator mass spectrometry

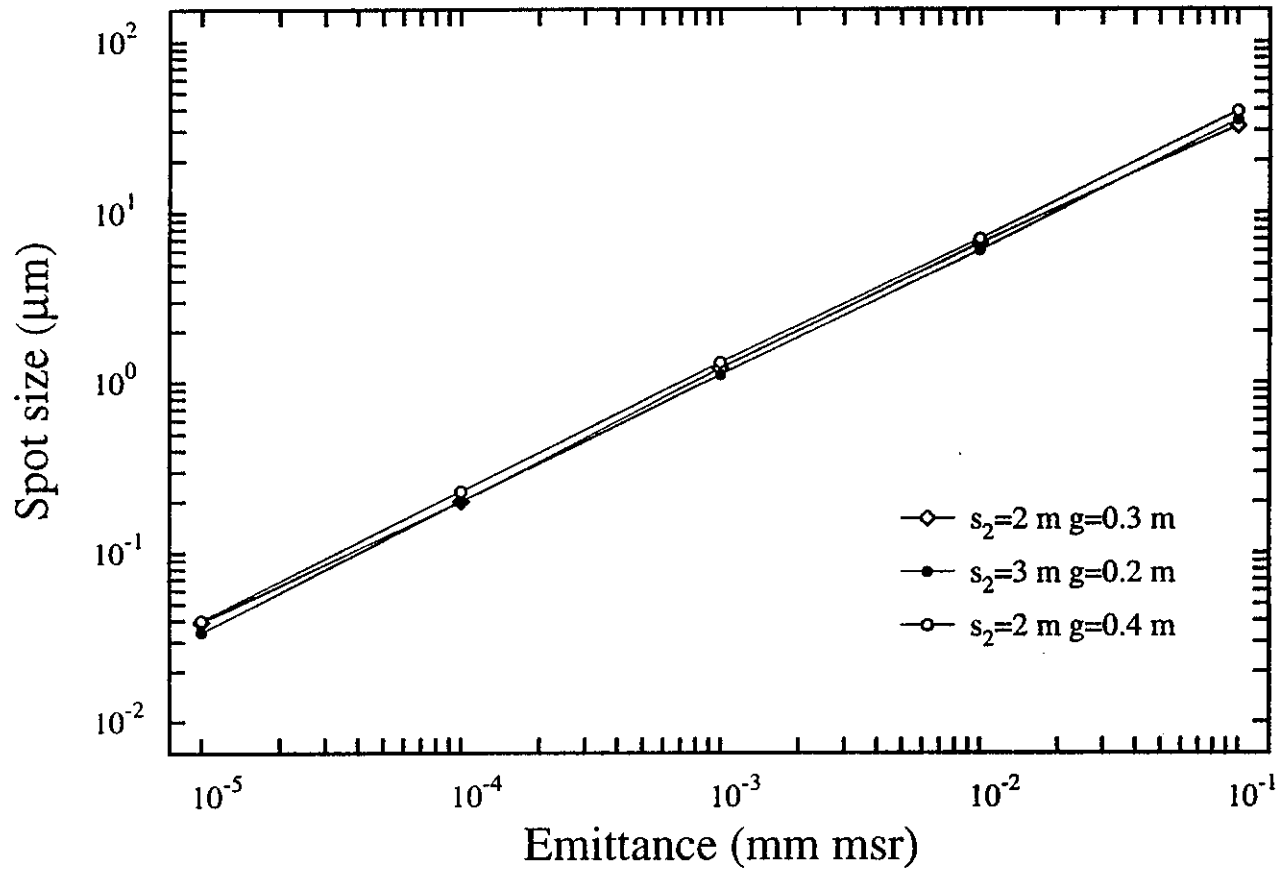

Figure 6: Dependence of the spot size versus emittance for various designs.

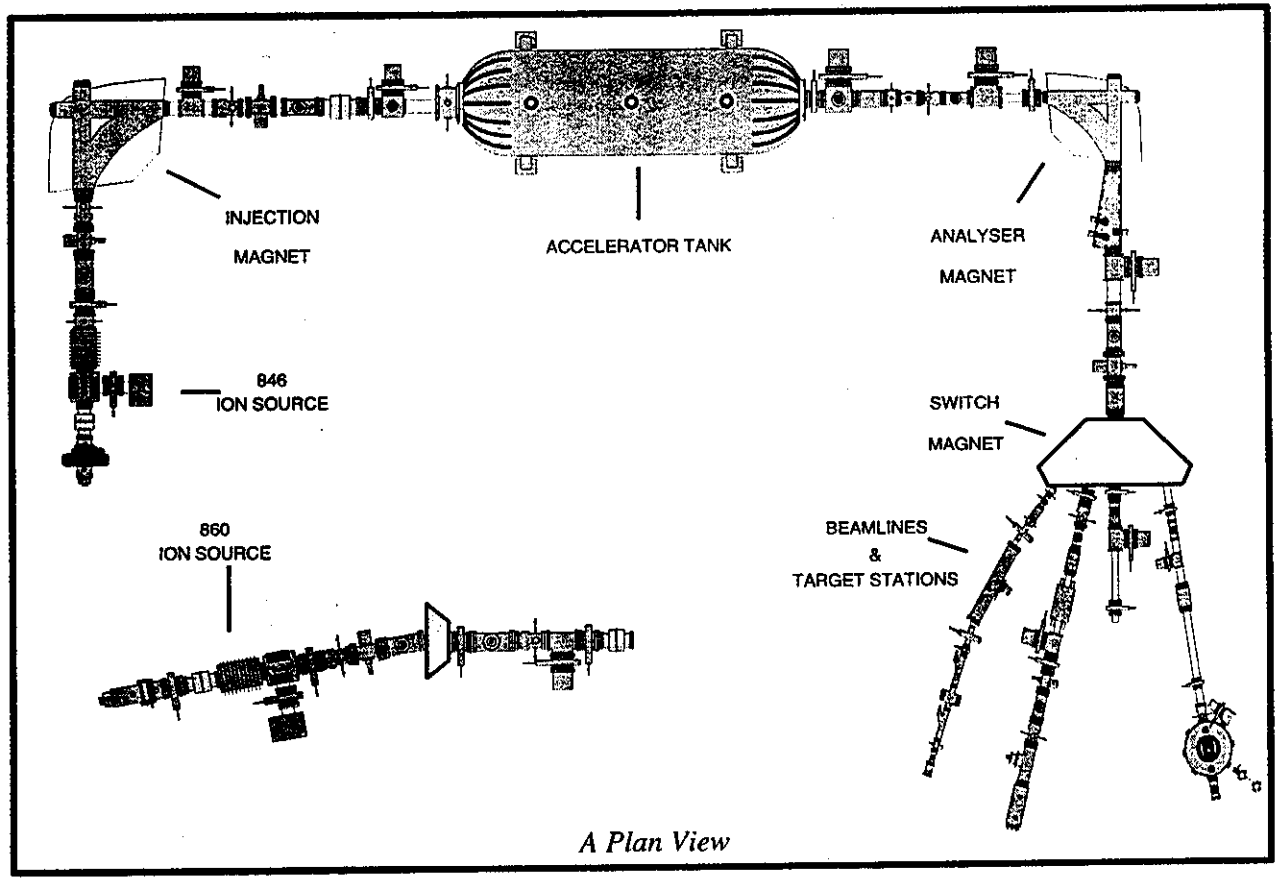

Figure 7: Beamline system at the ANSTO tandem accelerator.

(AMS), the IBA and the irradiation beamline. The proposed ion microprobe will be set up on one of the remaining free ports of the switching magnet.

The beam extracted from the tandem accelerator is mass analysed in a 90° magnet. The magnet has a mass energy product of 120 MeV amu/q^2. This is sufficient to bend the heaviest beams that will be used in the microprobe and it does not make sense to design a microprobe that exceeds the capabilities of this analysing magnet. After the analysing magnet the ion beam is distributed into the various beam lines by the switching magnet. The switching magnet has 14 ports between +65° and -65°. It has a mass energy product of 72 MeV amu/q^2 for the two 65° ports, while it is 120 MeV amu/q^2 or greater for all deflection angles up to 55°. This makes all, but the two 65° ports usable for the microbeam line.

A floor plan of the target area is shown in fig. 8. The floor plan shows that for angles greater than 45° there is at least 10 m space between the magnet and the wall, which should be enough to install a 6-8 m microbeam. However, it should be mentioned, that in our system in contrast to most microbeam systems, the beam has to pass through two magnets (i.e. an analysing and switching magnet), which will degrade the beam emittance.

In order to give an estimate on the performance of the proposed microprobe the beam brightness and the charge state distribution on the Tandem Accelerator were measured. As shown before, both parameter have a large influence on the performance of an ion microprobe.

4.7 Ion Beam Brightness

The beam brightness at the entrance of microprobe is the key factor for high currents on the target. To a first approximation the beam brightness is given by the ion source brightness. The ANSTO tandem accelerator is equipped with two sputter ion sources and a duoplasmatron source. With these ion sources, most elements of the periodic table are available as ion beams. The brightness of an ion source depends on the physical principles on which the source operates. In general rf or duoplasmatron ion sources are the brightest sources used on accelerators, with a brightness quoted between 5 and 13 μA/(mm^{2}mrad^{2}MeV).[43,51] New ion sources that are under current development such as the field ionisation source (FIS) or the liquid metal ion source (LIMS) have a brightness, which is 5 to 6 orders of magnitude higher. However, their use is limited, because of their short life times, of the order of some hours.

The high brightness sputter source 860 A from High Voltage on the ANSTO tandem accelerator is used for heavy ions. This sputter source has a normalized brightness of 0.2 μA/(mm^{2}mrad^{2}MeV), according to the specifications of the manufacturer, which is more then a factor of 10 lower compared to the brightness of an rf source.

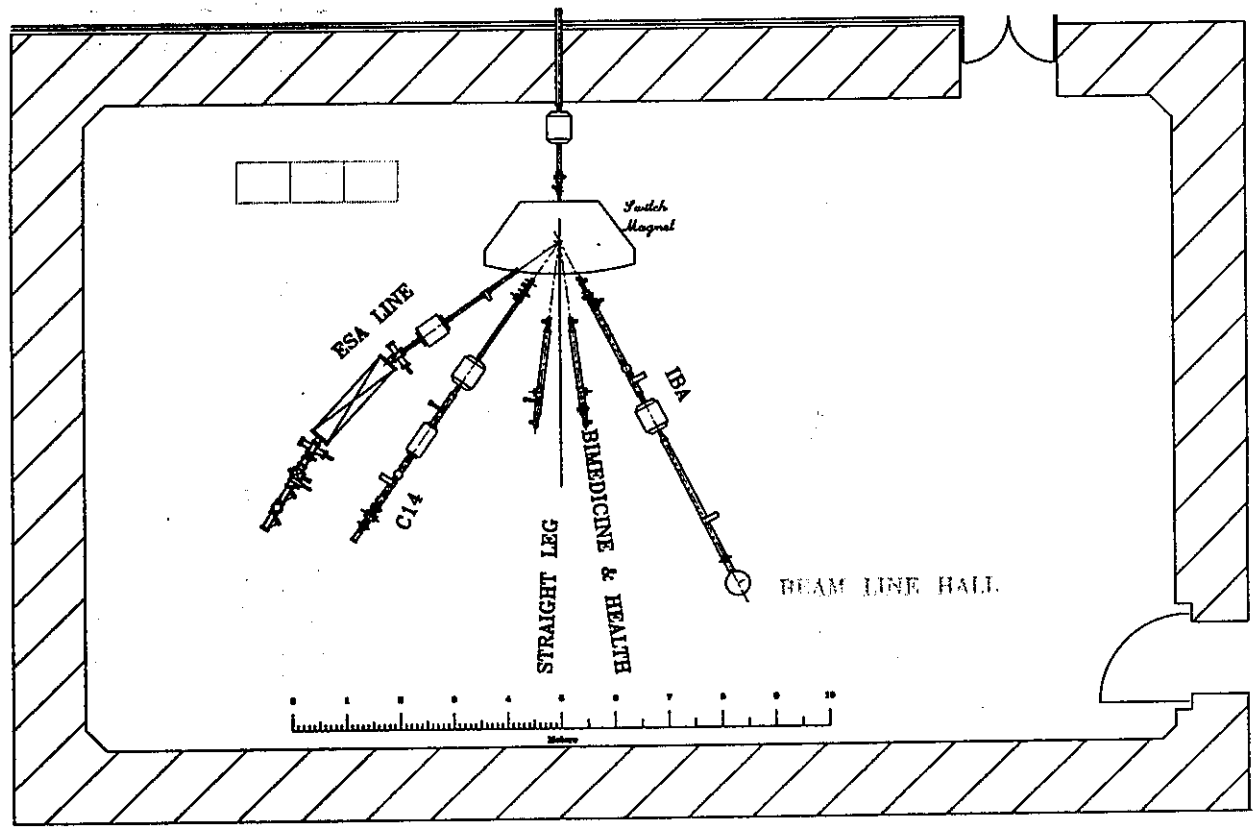

Figure 8: Floor plan of the experimental area at the ANSTO tandem accelerator.

The beam brightness in a tandem accelerator will further be degraded by the stripping process. As the beam of negative ions is stripped of electrons in the terminal the phase space occupied by the particles is increased and thus the brightness reduced. Meijer et al.[51] measured the brightness of their tandem accelerator to be 1.5 μA/(mm^{2}mrad^{2}MeV) for 3 MeV protons, which is about factor of 8 lower compared to that from a single ended machine. Grime and Watt[23] report an even larger degradation of the ion beam on their EN tandem accelerator at Oxford. The number of particles in the same phase volume is reduced by a factor of 50 by a gas stripper and a factor of 500 by a foil stripper. This leads to a reduction in brightness by the same factors.

The change in brightness caused by the stripping process depends strongly on the ions and the ion energy. The above examples are all given for protons for which the loss in brightness is expected to be less significant compared to that for heavier ions. On the other hand, the effect of the stripper is less severe at higher energies. For these reasons, brightness measurements are required in order to make reliable predictions on the target current.

In order to measure the beam brightness a 1 mm and 2 mm aperture were installed on the 55° beamline of the accelerator. Both apertures were 2 m apart, which defines an acceptance of 0.3536 mm mrad. From this acceptance and the beam current after the second aperture the brightness can be calculated. Faraday cups before and behind the first aperture allow the fine tuning of the beam through the first aperture. Due to the instability of the terminal voltage, the ion beam was moving across the first aperture, which made it very difficult to adjust the beam and pass it through the second aperture. Therefore the second aperture was later replaced by a Faraday cup, with a quartz window at the back. This allowed us to measure the beam current and the size of the beam spot simultaneously. The beam spot on the quartz viewer was then minimized and the size of the beam spot and the current recorded. From both values the beam brightness was calculated.

A series of brightness measurements was carried out at various beam energies and for different ions. As mentioned before; The stability of the tandem accelerator during the brightness measurements was very poor. Terminal voltage fluctuations were typically of the order of ± 5 kV, while under good conditions a stability of ± 1 kV is more typical. The reason for this instability of the tandem accelerator is unknown at this time. However, we are confident that it will be fixed in the near future. The terminal instability made the brightness measurements extremely difficult.

The results obtained underestimate the true brightness of the machine. The brightness of the accelerator at different terminal voltages is listed in the table 4. The brightness is given as a particle current rather than as an electrical current, because the particle current is the value that determines the feasibility of a technique. Besides the measured brightness the table contains an estimated value (in

Table 4: Results of the brightness measurements on the ANSTO tandem accelerator.

Ion	Term. Volt. MV	Energy MeV	EM/q^2	norm. Brightness μA/(mm^{2}mrad^{2}MeV)		Brightness μA/(mm^{2}mrad^2)
	foil stripping			measured	best	
C	5.0	25	18.8	$1.8*10^{-4}$	$1.3*10^{-4}$	$3.3*10^{-3}$
Cl	6.0	42	41.4	$2.3*10^{-6}$	$1.8*10^{-6}$	$8.0*10^{-5}$
I	6.5	65	101.9	$5.4*10^{-8}$	$6.2*10^{-8}$	$4.0*10^{-6}$
	gas stripping					
p	4.0	8	8.0	$9.0*10^{-4}$	$4.5*10^{-2}$	$3.4*10^{-1}$
C	6.5	26	34.7	$6.7*10^{-5}$	$6.4*10^{-4}$	$1.7*10^{-2}$
Cl	6.5	39	55.3	$3.0*10^{-5}$	$1.1*10^{-4}$	$4.3*10^{-3}$
I	6.5	65	101.9	$8.7*10^{-7}$	$6.3*10^{-5}$	$4.1*10^{-3}$

the column under best), which we believe should be achievable under more favourable conditions. The brightness was measured for both a gas and a foil stripping.

The results show two general trends. The beam brightness is higher for light ions than that for heavy ions, and the best results are achieved for gas stripping. Both results are expected, because of the change of the beam emittance during the stripping process at the terminal. The ions undergo small angular deflections during the stripping process, which increase the beam emittance and hence reduce the brightness. This small angle scattering increases with the square of the nuclear charge, thus effecting the brightness of heavier ion beam stronger than protons.

The highest brightness of $9.0*10^{-4}\mu$A/(mm^{2}mrad^{2}MeV) was measured for a proton beam at 4 MeV. However, under better conditions the brightness should be closer to $4.5*10^{-2}\mu$A/(mm^{2}mrad^{2}MeV). This is a factor of hundred lower than values conventionally achieved on single ended machines and it agrees very well with the decrease in brightness that is given by Grime and Watt.[23] However, this result is lower then the results given by Meijer et al.,[51] which show a 10 times higher brightness. However, their result was probably obtained with a duoplasmatron source, which is a brighter source in itself.

From protons to iodine the brightness is reduced by 2 orders of magnitude. This will reduce the beam current on target significantly for heavy ions. The brightness allows one to calculate a required system acceptance of the micoprobe system in order to achieve a target current of 100 pA. For protons a system acceptance of 0.0077 mm mrad is required, while it is 0.0343 mm mrad, 0.0682 mm mrad and 0.0698 mm mrad for C, Cl and I, respectively.

4.8 Charge State Distribution

The second parameter that is of importance for a microbeam operation is the charge state distribution of the ions extracted from the accelerator. A high charge state at a given beam energy is desirable, since this results in a lower value of the magnetic rigidity, which requires lower magnetic fields in the focusing quadrupoles.

The charge state distribution is a function of the terminal voltage, but also depends on the stripping medium. A foil stripper results in a higher charge state compared to that for a gas stripper, which would favour a foil stripper over a gas stripper in terms of the magnetic rigidity. However, this conflicts with the results of the brightness measurements which favour a gas stripper. Since the brightness has a much greater influence on the performance of the microbeam, gas stripping is the process that has to be used. The charge state distribution was measured for both stripping processes. Fig. 9 shows the results of the charge state distribution measurements. For comparison theoretical results for a foil stripper are shown.

4.9 Proposed Microbeam Design

Fig. 10 gives a schematic of the design proposed for the high energy, heavy ion microprobe. The microprobe consists of two high precision apertures. The first aperture is the so called object diaphragm (A_1), while the second is the aperture diaphragm (A_2). They are separated by the distance l_{12}. This defines the acceptance of the microbeam. Since slit scattering becomes a major contribution to the minimum spot size for small aperture sizes, the slits have to be carefully designed and manufactured with a high precision. In particular the surface roughness of the edges has to be minimized.

The two apertures are followed by an anti scattering aperture. This aperture can be of a more crude design. Its purpose is to stop particles scattered from the second aperture from reaching the lens system. Behind this aperture is the scanning system. This is required to scan the beam over an area of 1-2 mm across the specimen. Alternatively, the scanning system could be placed between the quadrupoles and the target. However, because of the constrains in space between the quadrupoles and the target it is often placed before the quadrupoles.

Following the scanning system are the beam focusing quadrupoles. Although a final decision about this system has yet to be made, a system consisting of two separate doublets is favoured at the moment. The configuration follows a design by A.D. Dymnikov[6,16] the inventor of the Russian quadruplet. It is a favourable optical system for heavy ion microprobes, since the two doublets act as two separate lenses. The total demagnification of the system is then the product of the demagnification of the two doublets. This allows demagnifications not achievable with a single lens systems, because of the limit in the magnetic field.

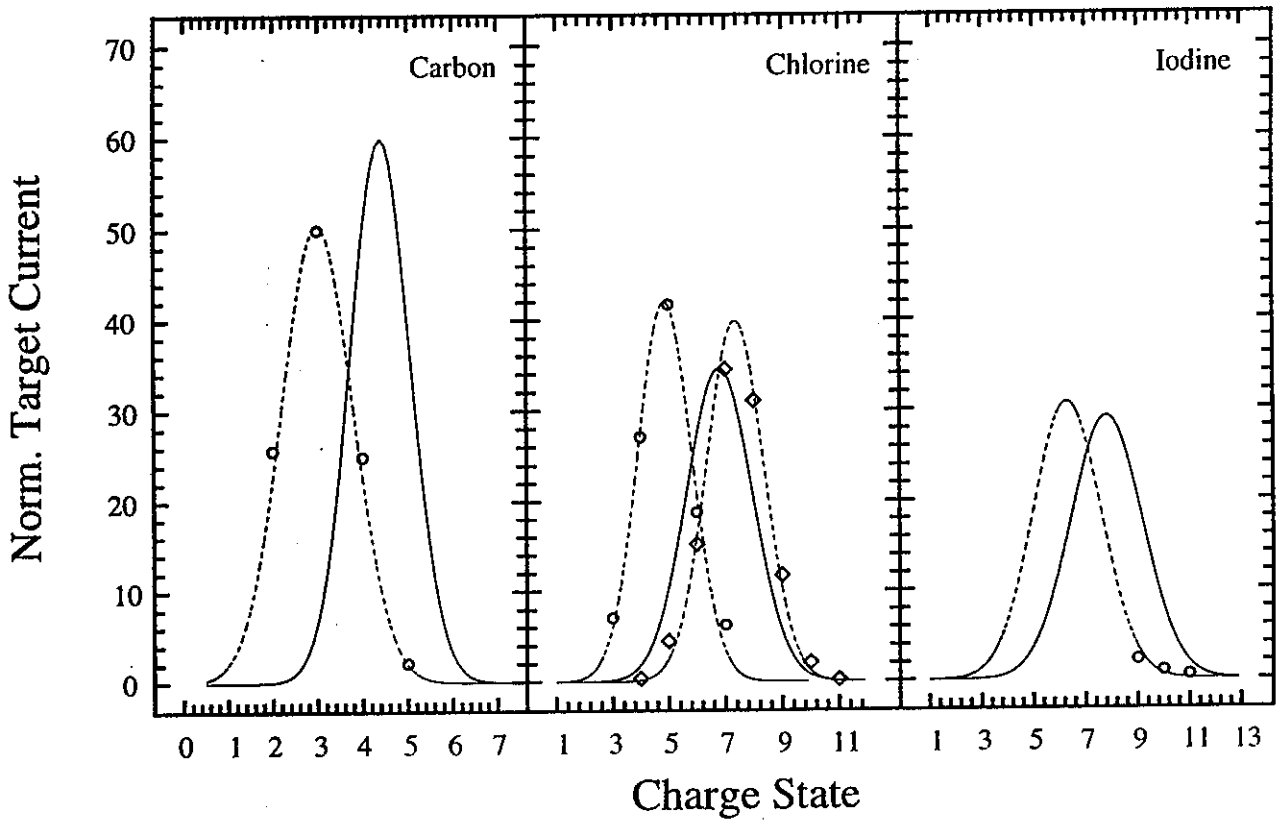

Figure 9: Charge state distribution of C, Cl and I. The Cl charge state distribution is given for a foil and gas stripper, while the C and I distribution are given for a gas stripper only. The solid lines are theoretical calculations, while the broken lines are included to guide the eye.

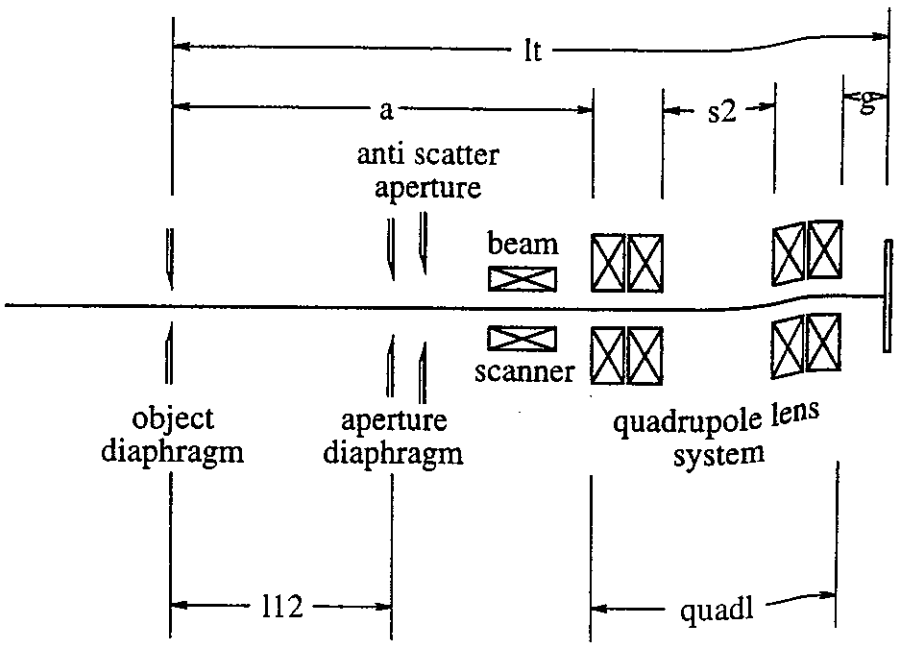

Figure 10: Schematic of the microbeam setup.

The placement and configuration of the lens elements in the quadruplet was optimized by a program written by Dymnikov,[17] that performs calculations on magnetic and electrostatic quadrupole lenses, taking into account aberrations up to 3rd order. The acceptance apertures are optimized to give a minimum spot size for a given acceptance.

The two quadrupole doublets are separated by the distance s_2 between 2-4 m. This large separation gives the heavy ion microprobe its unique properties. With this design, demagnifications between 10-30 can be achieved for heavy ion beams. This will result in beam spot sizes of a few microns in diameter.

Fig. 11 shows the beam envelope for one of the designs listed in table 5. The first two apertures limit the beam and thus defined the emittance, as can be seen by the change in the horizontal and vertical beam envelopes. The figure also shows the maximum spread in the lens system, which determines the minimum pole separation in the quadrupoles.

Table 5 summarizes the results of the calculations for various lens parameters of the quadrupole design. It must be pointed out, that the beam spot-size depends only on the geometry of the lens system and the acceptance of the ion microprobe. It does not depend on the beam energy or the ion species. The table shows a strong dependence of the beam spot size on variations of the emittance. Emittances below of 0.01 mm mrad and below are required for spot sizes well below 10 μm. Varying the geometry does not change the spot size much, however, the magnetic fields

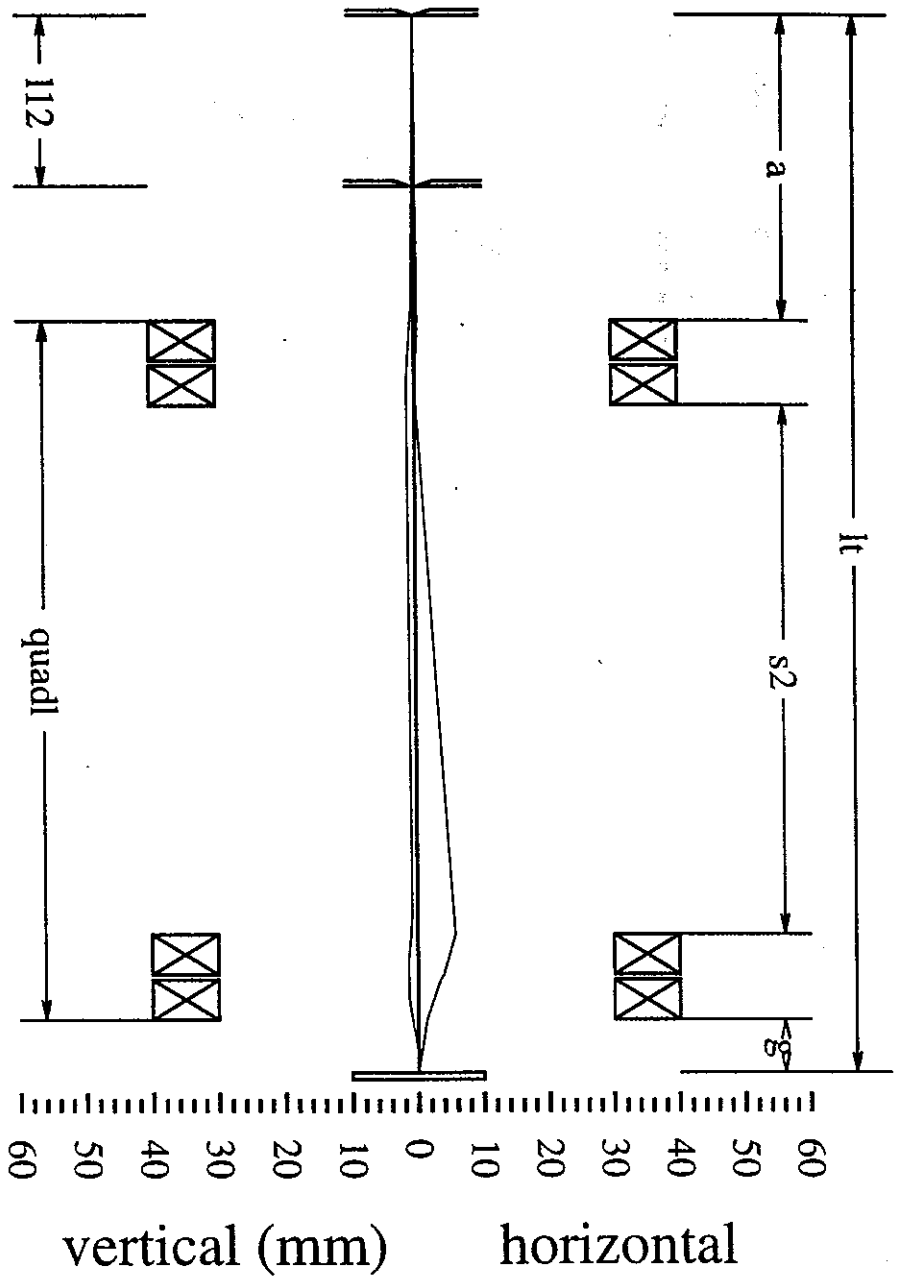

Figure 11: X and Y beam profiles.

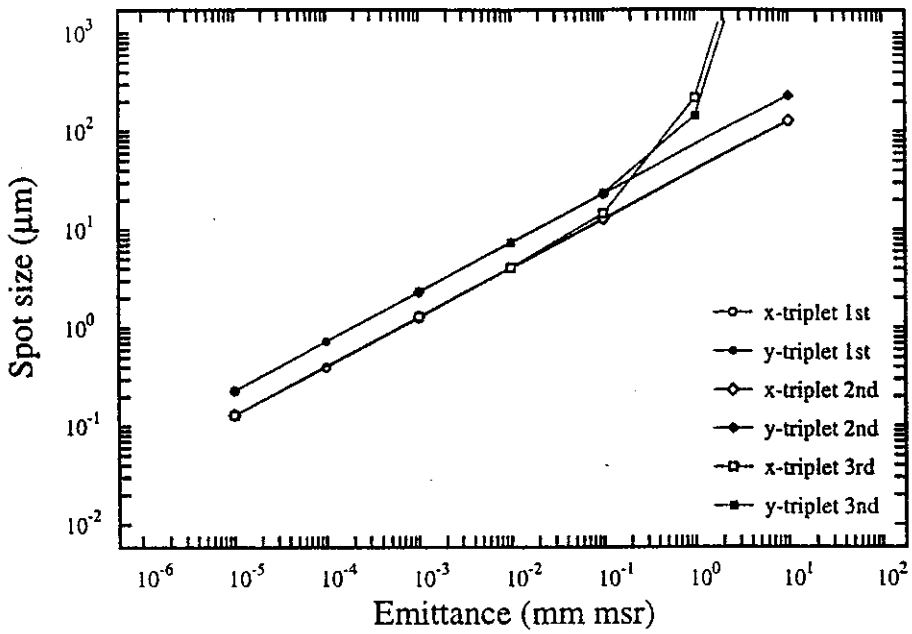

Figure 12: Dependence of the spot size versus emittance for a triplet design. The figure shows the first order spot sizes as well as the spot sizes including the second order (chromatic) and third order (spherical) aberrations.

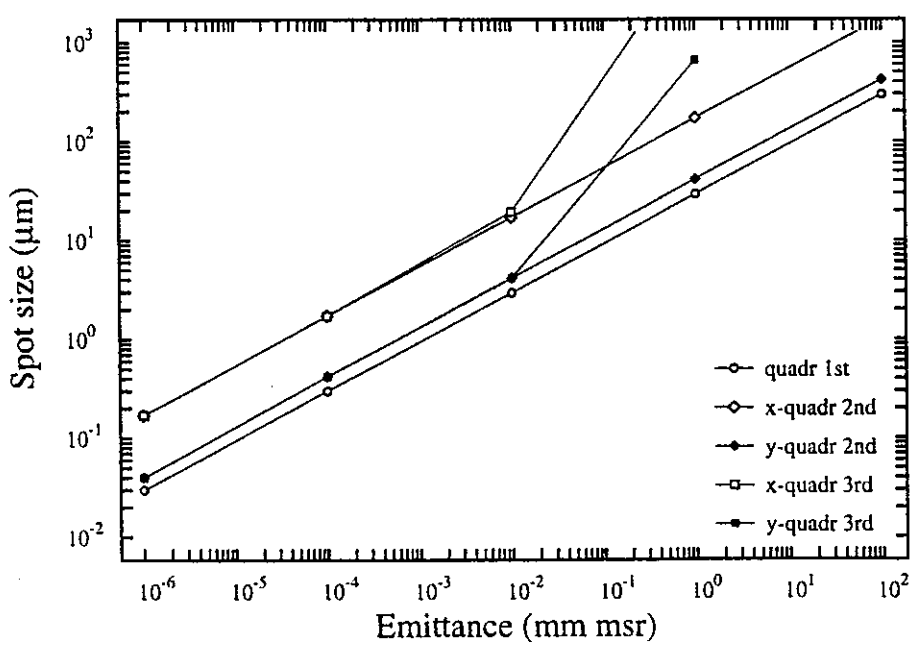

Figure 13: Dependence of the spot size versus emittance for a quadruplet design. The figure shows the first order spot sizes as well as the spot sizes including the second order (chromatic) and third order (spherical) aberrations.

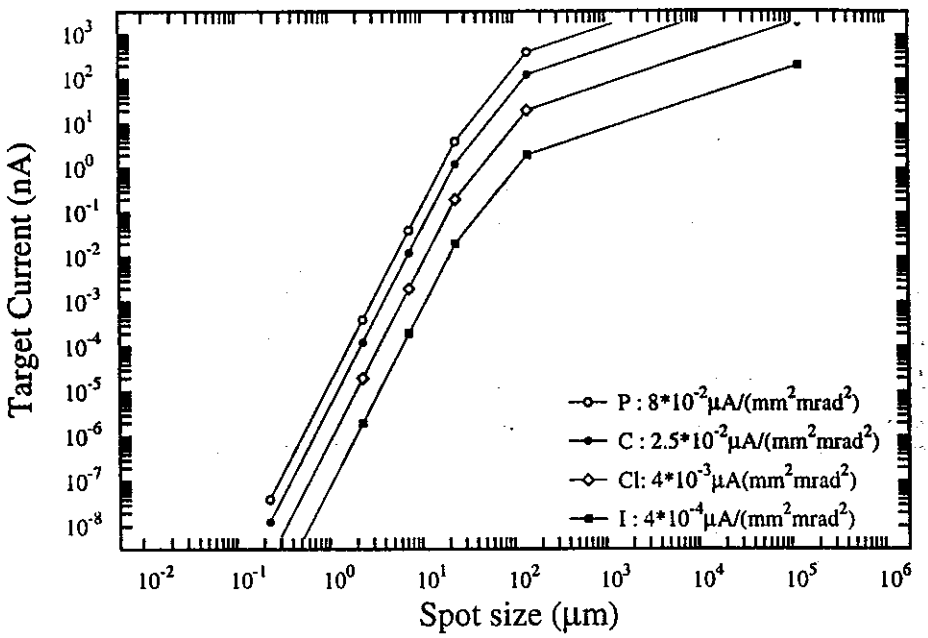

Figure 14: Dependence of the beam current on the spot size for various beam brightnesses. The figure shows the results for a typical triplet design.

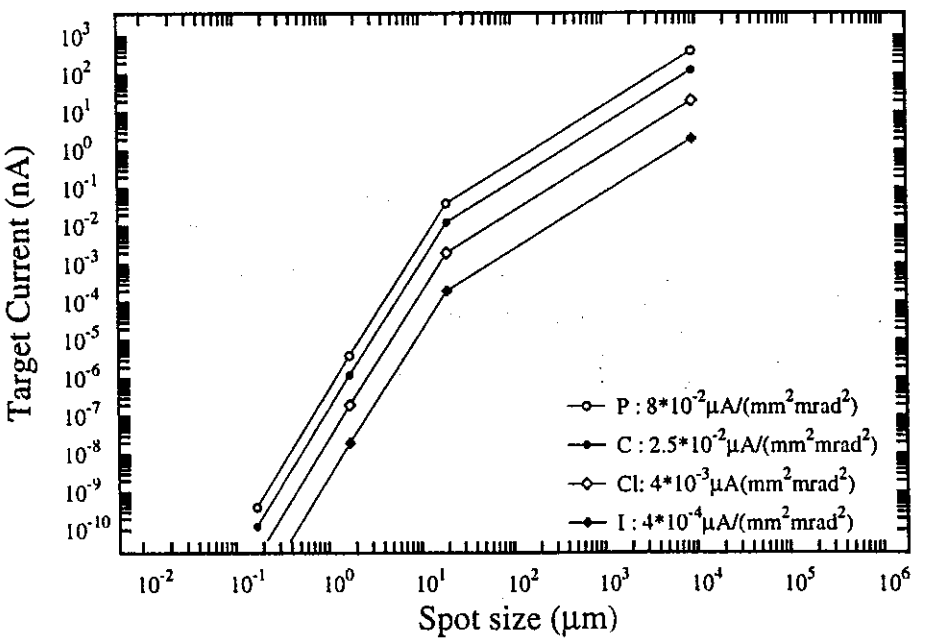

Figure 15: Dependence of the beam current on the spot size for various beam brightnesses. The figure shows the results for a typical quadruplet design.

Table 5: Summary of the calculations using the program written by Prof. Dymnikov. The table shows the magnetic fields required for a 90 MeV I^{11+} beam and a pole gap of 3 cm.

	Diam. μm	Emittance mm mrad	lens cm	s_2 m	g	l_{12} m	A_1 μm	A_2 μm	B_1 kG	B_2 kG	max. ME/q^2	D
1	6	0.01	30	3	0.4	1.3	150	275	3.0	1.9	95	22
2	7	0.01	30	4	0.4	1.3	100	475	2.9	1.9	101	18
3	7	0.01	30	2	0.3	3.0	175	650	3.7	2.1	62	31
4	7	0.01	30	2	0.5	1.3	125	450	2.9	2.0	101	17
5	7	0.01	40	2	0.4	3.0	150	825	2.3	1.3	161	23
6	14	0.01	30	3	0.4	1.3	300	500	3.0	1.9	95	22
7	15	0.01	30	4	0.4	1.3	250	625	2.9	1.9	101	18
8	15	0.01	30	2	0.3	3.0	425	850	3.7	2.1	62	31
9	16	0.01	30	2	0.5	1.3	275	600	2.9	2.0	101	17
10	17	0.01	40	2	0.4	3.0	330	1100	2.3	1.3	161	23

required change dramatically.

The magnetic fields required to focus an ion beam depends on the magnetic rigidity and it makes sense to use the maximum magnetic rigidity that can be focused at the maximum magnetic field strength of 3 kG as a figure of merit for a lens system, rather then comparing different ion beams. Hence, the maximum value for the magnetic rigidity ME/q^2 that can be focused properly with a 3 kG is given in the table as well. This is, besides the spot size, the most important parameter in the table, since it gives the range of heavy ion beams that can be focused.

The beam spot size and the magnetic rigidity are the most important parameters for the proposed microprobe, and the cases 5, 2, 4 and 1 have to be considered in the given order. By far the best configuration in terms of magnetic rigidity is case 5, which is due to the longer quadrupole lens length. However, it is not clear whether such a long lens can be build at affordable costs. Configurations with a short quadrupole separation s_2 and large aperture diameters A_1 and A_2 are preferred, because they make the alignment of the elements easier. This rules out the cases 2 and 4. After consideration of all advantages and disadvantages, case 1 of the table seems to be the best compromise. It will allow the to use of bromine at all energies and iodine up to 45 MeV.

However, the most important performance parameters of a microprobe are the minimum spot size and the achievable beam current. Both are related as mentioned earlier. For a given design the spot size can be reduced by reducing the emittance. This dependence between the beam spot size and the emittance is shown in fig. 6. The figure shows only marginal differences between different cases, which can

also be seen from the table 5. The graph demonstrates that it is, in principle, possible to achieve very small beam spot sizes by limiting the emittance. However, this results in very small beam currents on the target.

In order to verify these results, calculations with the Transport code[9] were carried out for the case 1. Fig. 13 shows the results obtained with the Transport-code. The results are in good agreement with the results obtained previously. However, it has to be pointed out that this code can not optimize for a minimum spot size, by varying the entrance apertures. The figure shows that the chromatic aberration and thus the energy instability of the accelerator has a significant influence on the minimum spot size, while the spherical aberrations only become significant at a larger emittance. This effect was not observed with the program written by Dymnikov (see fig. 6) and we suspect that this may be caused by numerical instabilities in the transport code. This suspicion is supported by the fact the spherical aberrations increase very strongly if the acceptance increases beyond a certain value.

As a comparison similar calculations were carried out using a simple triplet configuration. The results are shown in fig. 12. The first order spot sizes of this system are slightly larger than the spot sizes obtained with a quadruplet system. However, this system seems less sensitive to energy instabilities. In fact the spot size hardly changes at a $\frac{\Delta E}{E} = 10^{-3}$.

These calculations give a relation between the target current and the spot size for a given emittance. These results are shown in fig. 14 and 15. for the different brightnesses of P, C, Cl and I beams. From the figure, spot sizes for different target currents can be extracted. According to these calculations, a target current of 1 nA can be achieved for spot sizes somewhere between 10 and 100 μm. This is very promising considering that a target current of 1 nA is 10 time larger than the target currents generally used in proton microprobes.

4.10 Energy and Field Stability

The energy stability of the accelerator and field stabilities in the analysing and switching magnets have an influence on the minimum spot size and positional stability (both longitudinal and lateral). The energy stability for electrostatic accelerators is typically 0.025% - 0.05%. The stability of the FN-Tandem is around 1-3 kV, corresponding to 0.015-0.045% at 7 MV terminal voltage. Thus it is within the stability range of other accelerators used for microprobes. Instabilities of the magnet power supplies have a much smaller influence then terminal voltage instabilities. However, the power supply stability is far better than the energy stability of the accelerator and can therefore be neglected.

The magnetic field stability in the quadrupoles can also degrade the minimum spot size. The stability of the magnetic fields in the quadrupoles depends on the stability of the power supplies, for which stabilities of 10^{-5} can easily be achieved.

Power supply stabilities better than 10^{-4} are required to keep variations in spot size to tolerable values.

4.11 Precision of Mechanical Alignment of the Microprobe Elements

The importance of the alignment of the quadrupoles has been pointed out by various authors.[23,80] Traxel also mentions an increased spot size due to misalignment of the quadrupoles caused by material aging.

Grime and Watt[23] show scatterplots for various values of misalignments of the quadrupoles in different proton microprobe designs. Designs with quadrupole doublets and triplets prove to be the worst design case, hence the use of quadrupole quadruplets. In a quadrupole doublet design, a 1 mm misalignment leads to the loss of almost all focusing effects in one spatial direction. The quadrupole triplet is slightly less sensitive to misalignments. In terms of horizontal misalignments, the Russian quadruplet is the most stable design, the final alignment usually being done by minimizing the beam spot size. Usually a set of steerers is used to compensate for misalignment and an additional lens for a tilt. After the optimum spot size has been found the microprobe elements are moved until the same spot size is achieved without the use of the steerers and the extra lens. Therefore it is important to know how precisely the microprobe elements must be aligned. Various calculations of Grime and Watt[23] show that a precision of 0.1 mm is sufficient.

5 Detection Systems

Detection systems are of great importance, because the feasibility of an analysis technique on a microbeam depends on the count rate and one of the major factors determining the count rate is the detection solid angle Ω. In most ion beam analysis techniques the detection solid angle is in the order of Ω=1 msr. If it were possible to collect all particles or X-rays ejected in a backward direction (e.g. $\Omega=2\pi$) that would increase the count rate by 3 orders of magnitude. However, even a more modest increase of a factor of 10 reduces the required beam current significantly.

5.1 Elastic Recoil Detection

PIXE and ERDA are the most promising IBA techniques to use with an heavy ion microprobe. ERDA has the possibility to differentiate different elements in a sample by their mass or their nuclear charge. However, in order to separate different elements, multi-parameter detection systems are required. In principle two

different setups are possible, a time of flight system[49] or a combination of two detectors. In surface barrier detector heavy ions loose a significant fraction of their energy in nuclear collisions thus giving rise to the so called pulse height defect. Because of this pulse height defect, a time of flight ToF system is usually the better choice. Due to the long ToF, path in a ToF system the solid angles are very small, in the order of 1 msr.[49] Because the beam currents through the microprobe will be very small, a large solid angle Ω is required. A dE-E detection chamber with backgammon anode gives a solid angle as large as 7 msr and has therefore to be considered for microbeam applications. In ERDA, the particles are detected in a forward direction, therefore the focal length of the microprobe lens does not restrict the ERDA setup.

5.2 Backscattering and Nuclear Reaction Analysis

For Rutherford backscattering spectrometry a detector has to be placed in a backward direction between the target and the lens. An annular solid state detector that provides a large solid angle in the backward direction and additionally does not require very much space for mounting between the target and the lens is the preferred choice for RBS and NRA. This detector can also be used for nuclear resonances, which often have a maximum in the cross section in a backward direction.

Some nuclear reactions, however, are anisotropic with the maximum cross section not in the backward direction. Therefore an additional movable detector should be placed in the target chamber. This detector can also be used for RBS in a direction other than backward angles near 180°.

5.3 Particle Induced X-Ray Emission

PIXE is standard technique for elemental mapping with proton microprobes. However, its sensitivity for higher Z elements is limited by the fluorescent yields. PIXE using heavy ions particularly has an advantage for these elements, e.g. rare earth elements in geological applications.

The X-ray detector for PIXE is placed in a backward direction, between the target and the last quadrupole lens. In order to achieve a maximum solid angle it has to placed as close as possible to the target. A working length of the lens system between 30 and 40 cm provides sufficient room to place an X-ray detector.

5.4 Scanning Transmission Ion Microscopy (STIM)

A scanning transmission microscope can be operated in two different modes, in bright field or dark field mode. For bright field imaging a detector is mounted approximately 2-4 cm behind the target, with a collimator of 2-3 mm restricting the

angular acceptance range. This detector has to be accurately positioned vertically on the beam and has to be moved horizontally, perpendicular to the beam, over a several cm range.

For dark field imaging a second detector is mounted approximately 10-15 cm from the target on a manipulator that allows a vertical and horizontal position adjustment. A annular collimator restricts the detector to particles with small scattering angles.

Since the energy loss of a particle traversing through a target is measured as a function of the position, the particle detector with a good energy resolution are required. Both a detector a surface barrier detector (SBD) or a PIN photodiode fulfill these requirements and can be used.

5.5 Secondary Electron Imaging

The secondary electron rate as well as the energy spectrum of the electrons is characteristic for the material the ion beam is hitting. Therefore an image of a specimen can be created from the total electron flux. Since the total electron flux is very high the sample can be scanned very fast, which requires a very stable beam.[75] The majority of the electrons will have a low energy and only a small fraction created i.e. by an Auger process will have higher energies.

A channeltron electron multiplier is mounted in a backward direction. Secondary electrons with a few eV, are electrostatically extracted and accelerated to have sufficient kinetic energy when hitting the electron multiplier to produce a useful signal.

5.6 Ion Luminescence

It is well known that when an ion beam in the energy range of a few MeV/u impacts on a crystalline or organic sample, visible light can often be observed. This light is called ionluminescence (IL). The intensity of and the wavelength of the light can provide information about the nature of the luminescence centres, such as trace substituents and structural defects, found in the matrix. This makes IL a useful complement to other IBA methods, in characterizing e.g. geological specimens.[28]

The light produced by the specimen has to be collected by a lens system and goes through a window into the spectrometer. From the spectrometer it passes into a photomultiplier tube (PMT).

6 Summary

In summary the high energy heavy ion microprobe will be a new world class facility on the ANSTO tandem. Because of the higher energies on the FN tandem and the availability of heavy ions it allows a wide range of new applications. However, the most promising application are the use of ERDA, heavy ion RBS and SEU. ERDA and RBS allows depth profiling of elements, which was so far not possible on conventional light ion microscopes.

Ion beam imaging will be an other major topic for the microprobe. Because of the higher energy He ions available, they will have the same range as H ions used at conventional microprobes. Moreover the use of high energy He will enhance the contrast by more than a factor of 5 as compared to protons.

However, the most promising application is the use of the microprobe for SEU. The variety of ions over a wide range of energies available on the FN-tandem gives a huge variation in stopping power. This is import for various SEU studies. Together with a localized beam it allow to monitor radiation sensitive parts of devices.

References

[1] M. Ahmed et al., Nucl. Instr. and Meth. **B82** (1993) 584.

[2] W. Assmann et al., Nucl. Instr. and Meth. **B84** (1994) 726.

[3] P. Bayerl and P. Eichinger, Nucl. Instr. and Meth. **149** (1978) 663.

[4] F. Bosch, A. elGoresy, B. Martin, B. Povh, R. Nobeling, D. Schwalm, and K. Traxel, Nucl. Instr. and Meth. **149** (1978) 665.

[5] A.J.J. Boss, C.C.A.H. Van der Stap, R.D. Vis and H. Verheul, Nucl. Instr. and Meth. **B3** (1984) 654.

[6] V.A. Brazhnik, A.D. Dymnikov, D.N. Jamieson, S.A. Lebed, G.J.F. Legge, A.G. Ponomarev, and V.E. Storzhko, Nucl. Instr. and Meth. **B104** (1995) 92.

[7] M.B.H. Breese, G.W. Grime, and F. Watt, Nucl. Instr. and Meth. **B77** (1993) 169.

[8] M.B.H. Breese, G.W. Grime, and F. Watt, Nucl. Instr. and Meth. **B77** (1993) 301.

[9] D.C. Carey, K.L. Brown, and F. Rothacker, *Third-order transport, A computer program for designing charged particle beam transport systems* SLAC-R-95-462, Fermilab-Pub-95/0, UC-414.

[10] M. Cholewa, G.J.F. Legge, H. Weigold, G. Holan, and C. Birch, Nucl. Instr. and Meth. **B77** (1993) 282.

[11] G.E. Coote, Nucl. Instr. and Meth. **B66** (1992) 191.

[12] G.E. Coote and W.J. Trompetter, Nucl. Instr. and Meth. **B77** (1993) 501.

[13] W. Davison, G.W. Grime and C. Woof, Limnol. Oceanogr. **37** (1992) 1770.

[14] B.L. Doyle and N.D. Wing, IEEE Transactions on Nuclear Science **NS-30** (1983) 1214.

[15] B.L. Doyle, K.M. Horn, D.S. Walsh, and F.W. Sexton, Nucl. Instr. and Meth. **B64** (1992) 313.

[16] A.D. Dymnikov, D.N. Jamieson, G.J.F. Legge, Nucl. Instr. and Meth. **B104** (1995) 64.

[17] A.D. Dyminkov, Mathematica code for 3rd order quadrupole calculations [not published].

[18] C. Engelmann and J. Bardy, Nucl. Instr. and Meth. **218** (1983) 209.

[19] B.E. Fischer, Nucl. Instr. and Meth. **B10/11** (1985) 693.

[20] B.E. Fischer, Nucl. Instr. and Meth. **B30** (1988) 284.

[21] B.E. Fischer, Nucl. Instr. and Meth. **B54** (1991) 401.

[22] I.D. Gourlay and G.W. Grime, Int. Assoc. Wood Anatomists J. **15** (1994) 137.

[23] G.W. Grime and F. Watt, *Beam Optics of Quadrupole Probe-forming Systems* (Adam Hilger Ltd, 1984, Bristol).

[24] G.W. Grime and F. Watt, Nucl. Instr. and Meth. **B50** (1990) 197.

[25] G.W. Grime and W. Davison, Nucl. Instr. and Meth. **B77** (1993) 509.

[26] D.W. Heikkinen, G.S. Bench, A.J. Antolak, D.H. Morse, and A.E. Pontau, Nucl. Instr. and Meth. **B77** (1993) 45.

[27] F. Herrmann and D. Grambole, Nucl. Instr. and Meth. **B104** (1995) 26.

[28] N.P.-O. Homman, C. Yang, and K.G. Malmqvist, Nucl. Instr. and Meth. **A353** (1994) 610.

[29] Y. Horino, A. Chayahara, M. Kiuchi, K. Fujii, M. Satoh, and M. Takai, Jap. J. Appl. Phys. **29** (1990) 2680.

[30] Y. Horino, Y. Mokuno, A. Kinomura, A. Chayahara, and K. Fujii, Nucl. Instr. and Meth. **B100** (1995) 122.

[31] Y. Horino, Y. Mokuno, N. Tsubouchi, A. Kinomura, A. Chayahara, and K. Fujii, Nucl. Instr. and Meth. **B104** (1995) 49.

[32] K. Inoue, M. Takai, K. Matsunaga, M. Izumi, G. Gamo, and S. Namba, Nucl. Instr. and Meth. **B30** (1988) 580.

[33] T. Kamiya, N. Utsunomiya, E. Minehara, R. Tanaka, and I. Ohdomari, Nucl. Instr. and Meth. **B64** (1992) 362.

[34] A. Kinomura, M. Takai, K. Inoue, K. Matsunaga, M. Izumi, T. Matsuo, K. Gamo, S. Namba, and M. Satou, Nucl. Instr. and Meth. **B33** (1988) 862.

[35] F. Kraske et al. GSI-Preprint 89-70.

[36] J.P. Landsberg, B. McDonald, and F. Watt, Nature **360** (1992) 65.

[37] H.W. Lefevre, R.C. Connolly, G. Sieger, and J.C. Overley, Nucl. Instr. and Meth. **218** (1983) 39.

[38] H.W. Lefevre, R.M.S. Schofield, and D.R. Ciarlo, Nucl. Instr. and Meth. **B54** (1991) 47.

[39] G.J.F. Legge, C.D. McKenzie, and A.P. Mazzolini, J. Microsc. **117** (1979) 185.

[40] G.J.F. Legge, D.N. Jamieson, P.M.J. O'Brien, and A.P. Mazzolini, Nucl. Instr. and Meth. **197** (1982) 85.

[41] G.J.F. Legge et al., Nucl. Inst. and Meth. **B15** (1986) 669.

[42] G.J.F. Legge, Nucl. Instr. and Meth. **B22** (1987) 115.

[43] G.J.F. Legge, J.S. Laird, L.M. Mason, A. Saint, M. Cholewa, and D.N. Jamieson, Nucl. Instr. and Meth. **B77** (1993) 153.

[44] N.E.G. Lovestam, T. Calligaro, A. Duval, and J. Salomon, Nucl. Instr. and Meth. **B77** (1993) 66.

[45] M.J. McFarlane, D.J. Bowden, F. Watt and G.W. Grime, Contemporary leaching of the African erosion surface in Malawi, Mineralogical and Geochemical Records of Paleoweathering, eds. Schmitt and Gall, ENSMP Mem. Sc. de la Terre **18** (1992) 5.

[46] K.G. Malmqvist et al., Nucl. Instr. and Meth. **B77** (1993) 3.

[47] T. Matsukawa, K. Noritake, M. Koh, K. Hara, M. Goto, and I. Ohdomari, Nucl. Instr. and Meth. **B77** (1993) 239.

[48] F.W. Martin, Nucl. Instr. and Meth. **149** (1978) 475.

[49] J.W. Martin, D.D. Cohen, N. Dytlewski, D.B. Garton, H.J. Withlow, and G.J. Russel, Nucl. Instr. and Meth. **B94** (1994) 277.

[50] J. Meijer et al., Nucl. Instr. and Meth. **B89** (1994) 229.

[51] J. Meijer, A. Stephan, J. Adamczewski, H. Röcken, H.H. Bukow, and C. Rolfs, Nucl. Instr. and Meth. **B99** (1995) 423.

[52] J. Mesjasz- Przybylowicz, K. Balkwill, W.J. Przybylowicz, and H.J. Annegarn, Nucl. Instr. and Meth. **B89** (1994) 208.

[53] S. Metzger, J. Dreute, W. Heinrich, H. Rocher, B.E. Fischer, R. Harboe-Sorensen, and L. Adams, Proceedings RADECS 93.

[54] S. Metzger et al., IEEE Trans. Nucl. Sci. **41** (3) (1994) 589.

[55] Y. Mokuno, Y. Horino, A. Kinomura, A. Chayahara, M. Kiuchi, K. Fujii, and M. Takai, Nucl. Instr. and Meth. **B85** (1994) 741.

[56] Ph. Morretto, Y. Llabador, R. Ortega, M. Simonoff, and L. Razafindrabe, Nucl. Instr. and Meth. **B75** (1993) 511.

[57] Ph. Morretto, Y. Llabador, M. Simonoff, L. Razafindrabe, M. Bara, and A. Guiet-Bara, Nucl. Instr. and Meth. **B77** (1993) 275.

[58] Ph. Morretto, R. Ortega, Y. Llabador, M. Simonoff, and J. Benard, Nucl. Instr. and Meth. **B704** (1995) 292.

[59] D.H. Morse, G.S. Bench, S.P.H.T. Freeman, and A.E. Pontau, Nucl. Instr. and Meth. **B99** (1995) 427.

[60] J.C. den Ouden, A.J.J. Bos, R.D. Vis, and H. Verheul, Nucl. Instr. and Meth. **181** (1981) 131.

[61] A.E. Pontau, A.J. Antolak, and D.H. Morse, Nucl. Instr. and Meth. **B45** (1990) 503.

[62] V.M. Prozesky et al., Nucl. Instr. and Meth. **B104** (1995) 36.

[63] W.J. Przybylowicz, C.A. Pineda, V.M. Prozesky, and J. Mesjasz- Przybylowicz, Nucl. Instr. and Meth. **B104** (1995) 176.

[64] M.L. Roberts, G.S. Bench, D.W. Heikkinen, D.H. Morse, P.R. Bach, and A.E. Pontau, Nucl. Instr. and Meth. **B104** (1995) 13.

[65] H. Sayama, H. Kimura, Y. Ohno, S. Satoh, K. Sonoda, N. Kotani, and M. Takai, Jpn. J. Apll. Phys. **32** (1993) 6287, H. Sayama, M. Takai, H. Kimura, Y. Ohno, and S. Satoh, Scanning Microscopy **7** (1993) 825.

[66] R.M.S. Schofield and H.W. Lefevre, Nucl. Instr. and Meth. **B77** (1993) 217.

[67] R.M. Sealock, D.N. Jamieson, and G.J.F. Legge, Nucl. Instr. and Meth. **B29** (1987) 557.

[68] S.H. Sie and C.G. Ryan, Nucl. Instr. and Meth. **B15** (1986) 664.

[69] S.H. Sie, C.G. Ryan, D.R. Cousens, and G.F. Suter, Nucl. Instr. and Meth. **B45** (1990) 543.

[70] A. Stephan et al., Nucl. Instr. and Meth. **B89** (1994) 420.

[71] S.-A. Stuart, M. Cholewa, A. Saint, S. Prawer, G.J.F. Legge, and D. Weirup, Nucl. Instr. and Meth. **B77** (1993) 234.

[72] C.C. Sun, C.R. Lu, Z.Y. Fe, D.S. Yuan, Nucl. Instr. and Meth. **B40/41** (1989) 714.

[73] T. Sunde, J. Nystrom, and U. Lindh, Nucl. Instr. and Meth. **B54** (1991) 80.

[74] M. Takai, A. Kinomura, K. Inoue, K. Matsunaga, M. Izumi, K. Gamo, S. Namba, and M. Satou, Nucl. Instr. and Meth. **B30** (1988) 260.

[75] M. Takai, Y. Agawa, K. Ishibashi, K. Hirai, and S. Namba, Nucl. Instr. and Meth. **B54** (1991) 279.

[76] M. Takai, Y. Katayama, A. Kinomura, T. Lohner, S. Namba, and H. Ryssel, Nucl: Instr. and Meth. **B64** (1992) 277.

[77] M. Takai, Y. Horino, Y. Mokuno, A. Chayahara, M. Kiuchi, K. Fujii, and M. Satou, Nucl. Instr. and Meth. **B77** (1993) 8.

[78] M. Takai, Y. Katayama, T. Lohner, A.Kinomura, H. Russel, P.H. Tsien, E. Burte, M. Satou, and A. Chayahara, Rad. Effects and Defects in Solids **127** (1994) 357.

[79] T.A. Tombrella, in Materials Modifications by Energetic Ions and Atoms Eds.: K.S Grabowski et al. (MRS Symposium 1992) p273.

[80] K. Traxel, Nucl. Instr. and Meth. **A268** (1988) 567.

[81] K.Traxel et al., Nucl. Instr. and Meth. **B104** (1995) 19.

[82] R.D. Vis, J.L.A.M. Kramer, G.H.J. Tros, F. van Langevelde, and L. Mars, Nucl. Instr. and Meth. **B77** (1993) 41.

[83] R.L. Watson, C.J. McNeal, and F.E. Jenson, Advan. X-ray Anal. **18** (1975) 288.

[84] F. Watt, I. Orlic, K.K. Loh, C.H. Sow, P. Tong, S.C. Liew, T. Osipowics, T.F. Choo, and S.M. Tang, Nucl. Instr. and Meth. **B85** (1994) 708.

[85] C. Yang, N.P.-O. Larsson, E. Swietlicki, and K.G. Malmqvist, Nucl. Instr. and Meth. **B77** (1993) 188.

[86] C. Yang, N.P.-O. Homman, K.G. Malmqvist, J. Johansson, N.M. Halden, and V. Barbin, Scanning Microscopy **9** (1995) 43.